Dissertation

submitted to the
Combined Faculty of Natural Sciences and Mathematics of

Heidelberg University, Germany

for the degree of
Doctor of Natural Sciences

Put forward by

Daniel Bakucz Canário
born in: Lisbon, Portugal.

Oral examination: 16th June, 2021

Time Delay in Tunnelling Ionization

Referees: Honorarprof. Dr. Christoph H. Keitel
Prof. Dr. Björn Malte Schäfer

Abstract

A promising new method of attosecond spectroscopy, the attoclock, offers attosecond resolution without requiring attosecond laser pulses. However, it requires knowledge of the ionization time, opening up a long standing conceptual problem in physics ("how much time does tunnelling take?"). In this work, the time delay in the tunnel ionization process is considered. It is shown that a delay of the peak of the tunnelling wavefunction exists as a matter of principle, and is caused by the interference of transmitted and reflected components of the wavefunction. If sub-barrier reflections are neglected from the wavefunction, the delay in the peak vanishes and tunnelling is seen to be instantaneous. This is shown by considering a series of models of increasing complexity: the square barrier, an adiabatically tunnelling electron, and a wavefunction based on the Strong Field Approximation. This work has implications on the interpretation of atto-clock experiments: treatments based on instantaneous tunnelling should be adjusted in order to achieve appropriate calibration of the attoclock.

Zusammenfassung

Eine vielversprechende Methode ist die sogenannte Attouhr, die Attosekunden-Auflösung bietet, dabei aber auf die Verwendung von schwierig herzustellenden Attosekunden-Laserpulsen verzichtet. Hierzu ist allerdings die Kenntnis über den Zeitpunkt der Io-nisation erforderlich. Ist dieser bekannt, erhält man Zugang zu einem seit langem be-stehenden Problem der Quantenphysik: Wie viel Zeit benötigt das Tunneln. In dieser Ar-beit wird die Zeitverzögerung, die das Elektron während des Tunnel-Ionisationsprozesses erfährt, untersucht. Es wird gezeigt, dass diese Zeitverzögerung, eine durch die Poten-tialbarriere verursachte Verzögerung des Wellenpacketsmaximum, prinzipiell existiert. Dies wird anhand einer Reihe von einfachen Modellen mit zunehmender Komplexität diskutiert: eine konstante Barriere, ein adiabatisch tunnelndes Elektron und eine Wel-lenfunktion, die auf der Strong Field Approximation basiert. Weiterhin wird bewiesen, dass eine Vernachlässigung der Reflexionen an der Potentialbarriere dazu führt, dass die obengenannte Verzögerung verschwindet und das Tunneln instantan abläuft. Die-se Erkenntnis hat Auswirkungen auf die Interpretation der Attouhr. Beschreibungen, die auf instantanem Tunneln basieren müssen verbessert werden um eine korrekte Ka-librierung der Attouhr zu ermöglichen.

Contents

Chapter 1

Introduction

The study of material properties is a millennia old endeavour. In current times, this is done almost entirely through the study of the interaction of matter with electromagnetic (EM) radiation, predicated on the emission and absorption of light by atoms. Planck's seminal paper on the blackbody radiation spectrum introduced the revolutionary concept of discretizing the energy exchange between the blackbody and the EM field. This resolved not only the problem at hand but eventually led the way to Bohr's solution of the hydrogen spectrum and Einstein's theory of the photoelectric effect. The subsequent paradigm shift was later formalised in the 20th century into what is termed Quantum Mechanics.

One of the implications of the new theory was first grasped by Einstein as early as 1916 [1, 2], when he theorised the possibility of stimulated emission of coherent EM radiation via the newly discovered process of electronic energy level transitions. It was to take several decades and substantial theoretical and experimental effort [3] before Maiman and collaborators [4] finally constructed the first working laser in 1960. In the span of these few decades, lasers have become ubiquitous and are produced in a wide range of frequencies and intensities and having found countless applications.

One of the most desirable properties of lasers is their ability to focus near monochromatic light on very small areas, leading to large intensities. Following the invention of chirped pulse amplification by Strickland and Mourou [5], laser intensities have become so large that it is possible for laser light incident on a target to generate EM forces on orbiting electrons that are comparable to, or even greater than, their attraction to the nucleus, inducing controlled ionization of the atoms.

By way of example, the electric field experienced by an electron (of fundamental charge e and mass m_e) in the first energy level of the Bohr atom (with orbit radius

$a_B = \hbar^2/(m_e e^2))$ is given by $\mathcal{E}_a = e/a_B^2 \approx 5.1 \times 10^9$ V/cm, corresponding to an average intensity $\mathcal{I}_a \approx 3.5 \times 10^{16}$ W/cm^2 [6]. By contrast, the world's current strongest laser (ELI-NP, in Romania [7]) is scheduled to reach intensities of the order 10^{23} W/cm^2, many orders of magnitude greater than the characteristic atomic intensity, and more than capable of ionizing all known elements.

However, such immense intensities are not needed for ionization to take place. Were that to be the case, lightning would never strike as the field strengths[1] involved (of the order 10^3 W/cm^2) are far lower than those required for the electron to directly overcome the atomic barrier, a process known as over-the-barrier ionization (OTBI). In fact, at field strengths $\mathcal{E}_0$ below the OTBI threshold,

$$\frac{\mathcal{E}_0}{\mathcal{E}_{\text{th}}} \ll 1, \tag{1.1}$$

onization can still occur through one of two mechanisms. That is, via the absorption of multiple photons, thus granting sufficient energy for escape, or via tunnelling through the potential barrier generated by the combined atomic and electric potentials, a purely quantum mechanical process.

In a landmark paper [9], Keldysh was the first to identify these two mechanisms as limiting cases of the same non-linear theory of ionization. He established a parameter, eponymously known as the Keldysh adiabaticity parameter,

$$\gamma_K = \sqrt{\frac{I_p}{2U_p}} = \frac{\hbar \omega \kappa}{e \, \mathcal{E}_0}, \tag{1.2}$$

which defines the boundary between these two physical descriptions of ionization. It depends not only on the properties of the laser, such as the electric field strength $\mathcal{E}_0$, and frequency ω but also of the atom, namely the binding energy $I_p = \hbar^2 \kappa^2/(2m_e)$ and electron mass m_e. Its significance can be understood as follows.

When $\gamma_K \gg 1$, the energy imparted on an electron by the laser field (measured by the ponderomotive energy $U_p = e^2 \mathcal{E}_0^2/(4m_e \omega^2)$) is much smaller than the binding energy I_p, and so the ionization process is perturbative with respect to the field. If $\hbar \omega \ll I_p$ the atom may be ionised through electronic absorption of multiple photons of energy $\hbar \omega$. The probability of ionization then scales as $w \propto \mathcal{E}_0^{2n}$, where n is the number of absorbed photons. On the other hand, $\gamma_K \ll 1$ implies a slowly varying field, i.e. comparatively small ω and large $\mathcal{E}_0$, such that the electron experiences an essentially static strong field distorting the atomic potential and enabling the electron to quantum tunnel into the continuum. Consequently, the field effects are so large that ionization is seen to be a highly non-perturbative process, and the ionization rate scales as

$$w \propto \exp\left(-\frac{2\kappa^3}{3\mathcal{E}_0}\right). \tag{1.3}$$

---

[1] Using data from [8], measurements of the electric field strength of lightning show it to be of the order $\mathcal{E}_0 \propto 100$ kV/m, implying an intensity $\mathcal{I} \propto \varepsilon_0 c |\mathcal{E}_0|^2 \approx 10^3$ W/cm^2.

(a) Multiphoton Ionization   (b) Tunnel Ionization   (c) Over-the-barrier Ionization
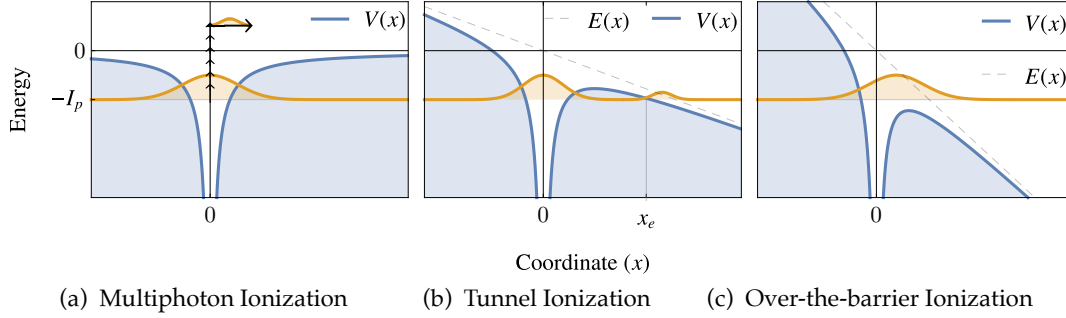
Figure 1.1: Schematic of ionization mechanisms, for the confinement of an electron wavepacket (orange) by a potential field (blue). For field strengths, $\mathcal{E}_0$, much smaller than the threshold filed strength, $\mathcal{E}_{\text{th}}$, the atom may be ionized by (a) absorbing multiple photons ($\gamma_K \gg 1$) or (b) tunnelling through the combined atomic and laser potential barrier ($\gamma_K \ll 1$). The coordinate x_e marks the continuum point of entry of the electron, where classically $x_e \approx I_p/(e\mathcal{E}_0)$. In the case $\mathcal{E}_0 > \mathcal{E}_{\text{th}}$, the barrier is lowered beyond the binding energy of the electron, allowing its escape (c) over the barrier (OTBI). Figure adapted from [10].

These are known as the *multiphoton* and *tunnelling* regimes, respectively, as pictured in Fig. 1.1. The Keldysh parameter may also be understood as a statement on the relative timescales between tunnelling and changes in the field, $\gamma_K = \omega\,\tau_K$. Here ω is the laser frequency and

$$\tau_K = \frac{\hbar\kappa}{e\mathcal{E}_0},\tag{1.4}$$

known as the Keldysh time, is the time taken for a classical electron to traverse the typical barrier distance $d \sim I_p/(e\mathcal{E}_0)$ with velocity of the order $v \sim \sqrt{I_p/m_e}$. Thus when $\gamma_K \gg 1$, the field oscillates at time scales much smaller than the typical time taken for tunnelling and vice-versa for $\gamma_K \ll 1$.

This simple description is able to explain many of the phenomena of strong field ionization. After ionisation through one of these mechanisms, the ionized electron will propagate in the electric field with limited influence from its parent ion. Depending on the properties of the laser field, the electron can either be carried off to a detector or be accelerated back toward the parent ion. In the latter case, it may either scatter from the ion, or recombine with the ion and in the process emit its laser acquired energy as a highly energetic photon (High Harmonic Generation, HHG [11, 12]), or even "kick out" other orbiting electrons from the ion (multiple ionisation, [13, 14]).

Phenomena such as HHG and multiple ionisation are not only interesting in their own right but can be used to characterise laser pulses and image atoms and molecules to very fine length and time scales. The orbital period of a ground state Bohr electron is of the order [15] of 150 attoseconds (1 as $= 10^{-18}$ s), so to study electron dynamics

in the time domain, attosecond resolution is required. However, the generation of such short pulses is experimentally challenging (although not impossible [16, 17]).

To overcome the need to generate such short pulses, a new attosecond spectroscopy method was developed which requires only femtosecond (1 fs= 10^{-15} s) pulses, and uses nearly circular elliptic polarization to imprint a finer time signature on the ionised electron. The rapidly changing ellipticity provides fine detail much like the seconds dial of a conventional clock, while the femtosecond pulse tracks longer time cycles like the minute or hour dial. This analogous working principle lends the technique the name of the *attoclock* [18–20].

Experimentally, the fs-laser pulse induces tunnel ionization and when the electron appears in the continuum, at the tunnel exit x_e at time t_0, its canonical momentum is given by

$$\mathbf{\Pi} = \mathbf{p}(t_0) + e\mathbf{A}(t_0), \tag{1.5}$$

where $\mathbf{A}(t) = \int_t^\infty \mathrm{d}t'\ \mathbfcal{E}(t')$ is the EM vector potential of the electric field $\mathbfcal{E}(t)$. The ionised electron and parent ion have opposite electric charges and so with an applied magnetic field around the reaction chamber they will be driven in opposite directions, where detectors may measure their individual momenta in coincidence, using a set-up known as "COLd Target Recoil Ion Momentum Spectroscopy" (COLTRIMS, [21]). The barrier through which an electron must tunnel is shortest at the peak of the electric field, meaning the probability of ionization is strongly peaked around the direction of the electric field peak, as given by the Keldysh ionisation probability, Eq. (1.3).

Since canonical momentum is a conserved quantity, and assuming no further effect from the parent ion on the ionized electron, the final electron momentum when detected at time t_f is given by $\mathbf{\Pi} = \mathbf{p}(t_f) = \mathbf{p}(t_0) + e\,\mathbf{A}(t_0)$. This follows from the observation that the vector potential is vanishing after the pulse has elapsed, $\mathbf{A}(t_f) \approx 0$. The final momentum, $\mathbf{p}(t_f)$, is experimentally determined and moreover the temporal profile of the vector potential $\mathbf{A}(t)$ is also known, so it is in principle possible to directly map electron momentum at the detector to electron dynamics near the atom. Since $\mathbfcal{E}(t)$, and hence $\mathbf{A}(t)$, are elliptically rotating fields, the preferred emission direction of the tunnelled electron also rotates, so electrons ionised at different times show up at different angles in the detector, as shown in Fig. 1.2.

The only inputs to this method are then the ionisation time, t_0, and momentum $\mathbf{p}(t_0)$, which must be physically estimated. Indeed, one of the first applications of the attoclock was exactly to experimentally determine the time taken in the tunnel ionization process. This would not only be of use to the attoclock method but also answer the fundamental question

"how much time does the tunnelling process take?"

While this simple question is tenable classically, it requires careful consideration when studying inherently non-deterministic quantum processes.

With classical energy conservation considerations, one expects the electron to ap-
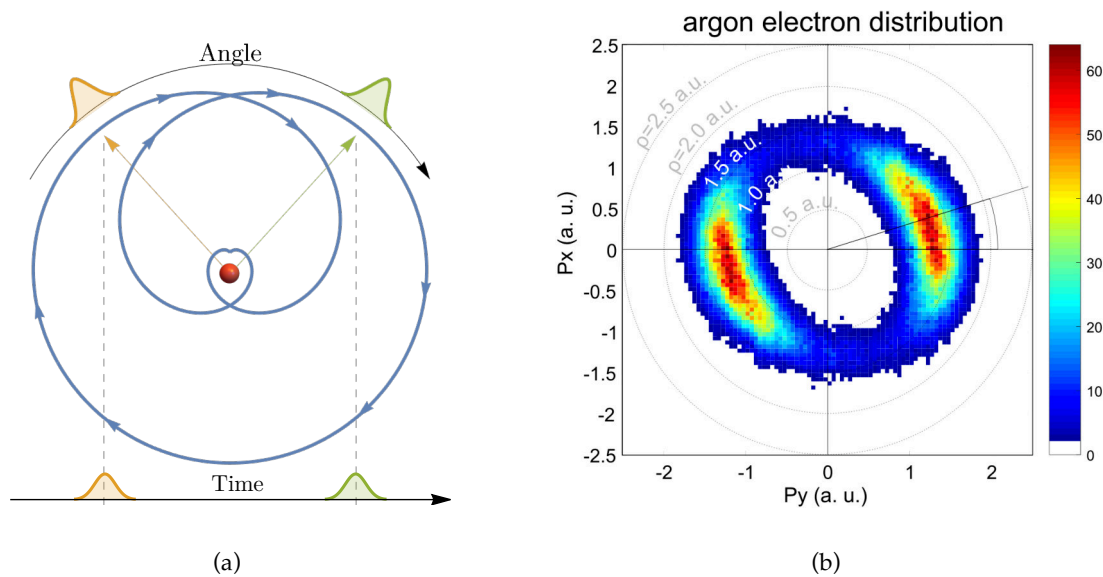
Figure 1.2: The attoclock (a) schematically and (b) experimentally. Panel (a) shows an end-on view of the elliptically rotating laser field (blue, arrows indicate increasing time) ionizing an atom (red). The tunnelled electron appears in the continuum and experiences a force perpendicular to the field. Electrons tunnelling at different times will be accelerated in different directions and be measured at different angles (adapted from [22]). Panel (b) is the experimental photoelectron momentum distribution (PMD), obtained by measuring the momentum of ionized electrons over several runs (reproduced from [23]). Without Coulomb or time delay effects the PMD is expected to be peaked at $\theta = 0$ w.r.t. the laser field, as this corresponds to the laser peak when the barrier is shortest and hence tunnelling is least suppressed. In reality, the experimental distribution is rotated by some angle which must be theoretically interpreted.

pear in the continuum with zero velocity, so that $\mathbf{p}(t_f) = e\mathbf{A}(t_0)$. However, if the tunnelling process is to take some time τ, one would expect the electron to arrive at a detector with momentum $\mathbf{p}(t_f) = e\mathbf{A}(t_0 + \tau)$. This would manifest itself experimentally as a rotation by some angle θ of the momentum angular distribution, as in Fig. 1.2, due to the time-to-angle mapping of the attoclock.

This theoretical analysis is based on the negligence of the effects of the long range ionic Coulomb field on the ionised electron. This effect, while small, is by no means negligible and consistently acts against the laser field, i.e. perpendicular to the final momentum $e\mathbf{A}(t_0)$, inducing a negative rotation of the momentum distribution.

Be that as it may, the classical premise of the above discussion is certainly not applicable to describe events surrounding the tunnelling process, which takes places at quintessentially quantum scales. These hurdles have led to a large [20, 22–35], and often contradictory, body of literature aiming to extract, or model, the relevant physical information from the attoclock. In particular, the debate is ongoing as to the existence

of this tunnelling time and what its meaningful definition may be. Direct experimental measurements are out of the reach with current technology but time delay and momentum around the tunnel exit have been investigated using virtual detector methods [36, 37].

The aim of this work is to clarify time delay concepts in ionization by analysing the process near the atomic core. This is done by constructing the wavefunction of the electron around the atomic core for physical parameters corresponding to tunnelling and observing the temporal delay of the peak in a series of models of increasing complexity. These range from simple textbook models of ionization to a fully quantum mechanical approach based on the Strong Field Approximation. The latter is applied first to a time independent laser field, with time dependence introduced later. It is shown that time delay, as defined by studying the peak of a tunnelling wavepacket, is generated by the interference of transmitted waves with waves being reflected from the edge of tunnelling barrier.

Emphasis is primarily placed on understanding the underlying physical concepts rather than accurately reproducing experimental results. These results, however, should influence future analysis of attoclock experiments as they show a clear need for quantum mechanical descriptions near the classically expected tunnel exit. Additionally, the methods employed in this work provide a new quantum mechanical estimate for the tunnel exit, based solely on properties of the wavefunction. This work thus opens potentially new ways to calibrate attoclock experiments other than the ill-suited classical picture outlined above.

This document is laid out as follows: Chapter 2 deals with the aspects of time measurement in quantum mechanics and introduces the Wigner time delay concept, applied extensively in later chapters. The origin of such a time delay is explained by the interference of transmitted and reflected components under the potential barrier. In Chapter 3 tunnelling ionisation is reviewed and the main theoretical concepts are introduced with a view to motivate this work. Chapter 4 presents the first model of ionisation, namely that of a constant laser field. By applying techniques of complex analysis to the wavefunction integral, the Wigner time delay in this case is shown to originate from the same interference principles. The techniques developed in doing so are then applied to a more realistic time dependent field in Chapter 5, where a pseudo wavefunction is constructed containing only transmitted components. This pseudowavefunction shows no time delay, establishing the principle that under the barrier reflections are causally linked to the Wigner time delay. This chapter is based, and borrows heavily from, the article [38]. Lastly, in Chapter 6, a model is considered where the tunnelling electron is allowed to rescatter from the atomic core and its influence on the Wigner time delay is tentatively analysed. In line with standards in atomic physics, atomic units, where $e = \hbar = m_e = 1$ are used exclusively hereafter. Conversion tables are available for reference in Appendix A.

Chapter 2

Time Delay

The passage of time is a familiar concept, permeating our experience and description of physical processes. At a most basic level, time is the measure of change between consecutive events or states. Seen through this lens, time is seen to always be linked to some dynamical variable, for example a coordinate or energy change. Time itself, however, is no dynamical variable. To paraphrase Peres [39], it makes no sense to talk of a particle with a well defined time, t. Time is merely a book keeping device. In classical mechanics, time assumes this role as a mere parameter evolving the relevant physical fields via the equations of motion. Even relativistic and gravitational mechanics, which formalised the link between time and dynamical variables by elevating time to a fourth coordinate, treat time as parametric[1].

The guise of time in quantum theory however, is not at first obvious. In his seminal papers on a quantal wave theory, Schrödinger first derived [40] a time independent equation for stationary states and only later was a time dependent formulation introduced (arguably [41, 42] using semi-classical principles). In the new theory, since the dynamical variables became non-deterministic, quantum mechanical definitions of time (and measurements thereof) turned themselves inherently non-deterministic. Despite the conceptual difficulties involved, techniques to measure time quantum mechanically have been developed, albeit each with its nuances (see e.g. [43] for a complete and historical survey).

Of particular interest is the question: "how much time elapses during a state transition?" In other words, are "quantum jumps" instantaneous, and if not, how long do they last? Closely related to this question, and forming one of the central ideas of this thesis, is the question "is quantum tunnelling an instantaneous process?" As will be shown, these questions are somewhat of a red herring but nonetheless, strongfield ionization is well suited to shine light[2] on them. The purpose of this chapter is to provide a

---

[1] All these theories stand in stark contrast to classical thermodynamics, where the Second Law establishes a fundamental link between the arrow of time and increases in entropy. Ironically, it was exactly the failure of thermodynamics in accurately describing the blackbody radiation spectrum that ushered in quantum mechanics, where the arrow of time assumes relevance in the study of open quantum systems.

[2] No pun intended.

flavour of tunnelling time procedures and to introduce a measure which is extensively used in studies of strong field tunnelling ionisation, viz. the Wigner time.

To provide a simple framework the case of tunnelling through a box potential is presented. Within this context, the emergence of a Wigner tunnelling time is shown to be caused by the interference of waves reflected by the boundaries of the box potential with those of the transmitted waves. This principle is a fundamental to this work and will be applied to more sophisticated models of ionisation in later chapters.

2.1   Tunnelling Times

Theoretical measures of tunnelling time can be broadly divided into types: time-of-passage methods and dwell times. As the names imply, while passage times aim to measure the time associated with passage of wavepacket as it traverses the barrier, dwell times aim to quantify how much time on average a particle spends in the barrier region. However, all measures utilise features from the transmission wavefunction ψ and potential V. In what follows, four related concepts of tunnelling time are presented along with their relative limitations. For interesting discussions of tunnelling times within the context of strong field ionisation see e.g. [27, 32, 34]

The Larmor Clock

The Larmor clock, introduced by Baz [44] and Rybachenko [45] in the 1960s, leverages the fact that an electron spin precesses in the presence of a magnetic field, B. By preparing an electron in a given spin state and applying a weak magnetic field across the barrier region, say in the vertical z direction, the electron spin will rotate in the $x - y$ plane by the angle

$$\theta = \omega_L \, \tau_L \tag{2.1}$$

where $\omega_L = -B/2$ is the Larmor frequency (in atomic units) and τ_L, the Larmor time, is the time of the spin-magnetic-field interaction. Therefore, one can map the angle of precession directly to the duration of the interaction (.i.e. the time of passage through the barrier).

Büttiker [46], however, noted that such a barrier was asymmetric with regards to spin up and down states. Spin polarization along the x axis can be represented as an equiprobable mixture of spin up and down polarizations in z and so spins aligned with the magnetic field have lower energy and experience a lower potential barrier and are thus preferentially transmitted. This causes a small spin rotation in the direction of the magnetic field with a new associated measure of time to this rotation, τ_z, determinable by the fact that

$$\langle s_z \rangle = \frac{1}{2} \omega_L \tau_z \tag{2.2}$$

where $\langle s_z \rangle = \frac{1}{2} \langle \psi | \sigma_z | \psi \rangle$ is the spin expectation value for the transmitted component. Recently, the Larmor clock principle found its first experimental application [47]: using a pseudo-magnetic field (a two-level system in a resonant laser field where energy states act as spin states) the tunneling of rubidium atoms through an optical barrier was investigated, finding a Larmor traversal time in the order of miliseconds. Unfortunately, the need for the preparation of a magnetic field across the barrier limits its application to ionization problems.

Büttiker-Landauer Time

In order to study material properties where tunnelling was a relevant physical process, Büttiker and Landauer [48] considered tunnelling through a time dependent barrier with a small perturbation $V(x,t) = V_0(x) + V_1(x,t)$, where $V_0 \gg V_1$. In their framework, they deduced a measure of the time for tunnelling to be

$$\tau_{BL} = \int_{x_1}^{x_2} \mathrm{d}x \, \sqrt{\frac{m}{2(V_0(x) - E)}}, \tag{2.3}$$

where x_1, x_2 are the classical turning points for a particle with mass m and energy E in the potential $V_0(x)$. Of particular interest is the fact that this measure can be used as a parameter to identify two limiting cases of tunnelling, depending on the frequency ω of the time dependent perturbation V_1. They note that for high frequencies, tunnelling is enhanced by absoprtion of photons of energy $\hbar\omega$ and for low frequencies, the potential is essentially static with respect to the tunnelling timescale.

This is in exact equivalence to the Keldysh parameter, τ_K, introduced in Eq. (1.4), which serves the same purpose in the study of ionization. The two can be understood as a measure of the formation time of a tunnelled wavepacket, i.e. the minimum interval in time necessary to describe the creation of a wavepacket outside the barrier. While related, this is a different concept from that of the time *delay*, which describes the relative hindrance of the wavepacket due to the barrier.

The Feynman Path Integral

The Feynman Path Integral (FPI) formalism [49] can also be used to understand how much time, on average, a particle spends inside the barrier. The wavefunction in FPI formalism is defined by

$$\Psi(x,T) = \int \mathrm{d}x_i \int_{x_i(0)}^{x(T)} \mathcal{D}x \, e^{i\, S(x(t))} \, \psi(x_i, 0) \tag{2.4}$$

where the measure $\mathcal{D}x$ runs over all trajectories $x(t)$ starting from x_i at time 0 and ending at position x at time T. The FPI can be seen as a weighted sum over all paths $x(t)$, where the weighting factor is the classical action under a potential V:

$$S(x(t)) = \int_0^T \left(m\dot{x}^2/2 - V(x) \right) \, dt. \tag{2.5}$$

The tunnelling time in the FPI framework can be understood by analysing the portion Φ of paths that spend some time inside the barrier, and so is the FPI is well suited to study the dwell time. Given a time τ, the subset of paths spending exactly τ units of time inside the barrier region, Ω, is given by

$$\Phi(x, T | \tau) = \int \mathrm{d}x_i \int_{x_i(0)}^{x(T)} \mathcal{D}x \, \delta \left(t_\Omega(x(t)) - \tau \right) \, e^{i \, S(x(t))} \, \psi(x_i, 0) \qquad (2.6)$$

where $t_\Omega(x) = \int_0^T \Theta(x(t))$ is a clock measuring the time spent by the particle inside the barrier (Θ_Ω is a Heaviside step function with value unity whenever $x(t) \in \Omega$ and zero otherwise). While the formalism casts the tunnelling time problem in very natural language, it suffers from a significant malady. Yamada [50] pointed out that no probability distribution for the times τ using the FPI can be meaningfully defined. In his own words, the failure to satisfy this condition means

> "*different τ's represent interfering alternatives to a particle, just as the two alternatives do in the two-slit experiment. Because of temporal interference, we cannot consider that a particle spends a certain amount of time in the barrier with some probability, just as we cannot consider, due to spatial interference, that it passes through either slit with some probability.*"

The work around this complication is to consider ranges of values of τ and determine the probability distribution of the different ranges, a technique known as "coarse graining". Like the other techniques described here the FPI is not perfect but its applications to ionisation times may also be found in [27, 34].

The Eisenbud-Wigner-Smith Time

One other very common method used to study time in quantum mechanics was proposed by Eisenbud [51] and his supervisor Wigner [52, 53] in the context of s-wave scattering. A decade later, Smith [54] used similar reasoning to define the concept of *collision lifetime*. The central tenet of their method is that the scattering centre disturbs the wavefunction ψ, having an effect on the group velocity of the scattered wavepacket, which affects the peak of the distribution. Mathematically, this effect can be measured by tracking the changes of the wavefunction phase φ with respect to the energy E

$$\tau_W(x) = -i \, \frac{\partial \varphi}{\partial E} = -i \, \frac{\partial}{\partial E} \ln \frac{\psi(x)}{|\psi(x)|}. \qquad (2.7)$$

Physically, the EWS time (Wigner time for short) can be understood as the tracking of the peak of the wavefunction as it crosses the potential. Since the momentum space electron wavepacket in a typical attoclock experiment is well defined, as seen in Fig. 1.2 (b) of Chapter 1, it is an oft used tool in the strong field laser community for the study the electron time delay. It is, however, not without its drawbacks. Crucially, the Wigner
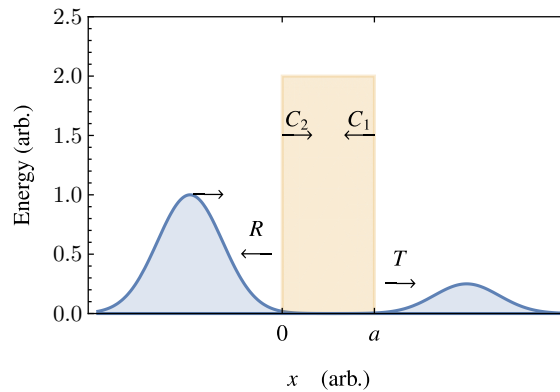
Figure 2.1: Schematic of the scattering of wavepacket by a square barrier potential (not to scale). The dynamics of the wavepacket are governed by the piecewise solution of the Schrödinger equation for the three regions shown, given by Equations (2.9)-(2.10), for each frequency.

time measures the *delay* a wavefunction experiences due to the influence of the potential, compared to its unimpeded motion. For polychromatic wavepackets, a potential barrier will preferentially transmit higher energy components, potentially leading to negative time delays (undesirable for a measure of interaction time). Thus, it is suitable for use with sharply peaked wavepackets, where meaningful conclusions can be drawn, as is the case for tunnelling ionization [19, 20, 24].

2.2   Scattering of a Wavepacket by a Box Potential

Having introduced some aspects of the time delay problem, this section deals with deriving the measure most commonly used in studies of strong field ionization, namely the Wigner time. As discussed in Chapter 1, one of the pieces of information necessary for the analysis of attoclock data is information on the appearance of the electron in the continuum. By following the phase of the transmitted wavefunction, the Wigner time can provide information on the appearance in the continuum of the peak of the wavefunction, which can be used to untangle the contributions to the attoclock rotation angle. This is of particular importance as Coulomb field effects manifest themselves in the photoelectron momentum distributions in a similar way to time delay effects.

The Wigner time is derived here for the special case of a constant potential barrier, following in the style of Bohm's classic textbook [55], which highlights the necessary concepts for later chapters. In addition to this, the emergence of this Wigner time delay as a consequence of interference effects is shown for this case. This will be a recurring theme throughout later chapters, culminating in its application the strong field ionization problem.

Begin by considering a wave packet

$$\Psi(x,t) = \int \mathrm{d}p \, f(p - p_0) \, \psi(p) \, e^{-i \, E(p) \, t} \tag{2.8}$$

with energy $E(p) = p^2/2$, incident on a potential barrier $V(x) = V_0$ for $0 \leq x \leq a$ and 0 elsewhere, where $f(p - p_0)$ is some distribution peaked at p_0 (e.g. a Gaussian). This setup is sketched in Fig. 2.1. Each p-component wavefunction obeys the time-independent Schrödinger equation with the piecewise solution

$$\psi_I(x) = e^{ipx} + Re^{-ipx}, \tag{2.9}$$
$$\psi_{II}(x) = C_1 e^{qx} + C_2 e^{-qx}, \tag{2.10}$$
$$\psi_{III}(x) = Te^{ipx}, \tag{2.11}$$

with momenta $p = \sqrt{2\,E}$ and $q = \sqrt{2(V_0 - E)}$. The amplitude of the incoming wave has been set to unity, without loss of generality, and the co-efficients C_1 and C_2 are the typical reflection and transmission coefficients under the barrier, respectively.

Matching the above solutions and their derivatives at the boundaries yields the coefficients

$$C_1 = \frac{(-2i\chi)(1 + i\chi)e^{-\xi}}{(1 - i\chi)^2 \, e^{\xi} - (1 + i\chi)^2 \, e^{-\xi}}, \tag{2.12}$$

$$C_2 = \frac{(-2i\chi)(1 - i\chi)e^{+\xi}}{(1 - i\chi)^2 \, e^{\xi} - (1 + i\chi)^2 \, e^{-\xi}}, \tag{2.13}$$

$$R = (1 + \chi^2) \, \frac{e^{-\xi} - e^{\xi}}{(1 - i\chi)^2 \, e^{\xi} - (1 + i\chi)^2 \, e^{-\xi}}, \tag{2.14}$$

and

$$T = \frac{(-4i\chi)e^{-ipa}}{(1 - i\chi)^2 \, e^{\xi} - (1 + i\chi)^2 \, e^{-\xi}}. \tag{2.15}$$

The dimensionless parameters $\chi = p/q$ and $\xi = q\,a$ have been introduced, whose role, loosely speaking, determines the relative length and height of the barrier respectively.[3] The problem is thus solved for any choice of barrier height χ, length ξ and frequency p. In what follows, we aim to determine the effect of the tunnelling on the wavepacket motion.

---

[3]When $\chi \to \infty$ then $q \ll p$ from which it follows $E \gg V_0/2$. This corresponds to a barrier where the energy is on the order of the potential height, that is a low barrier. Conversely, $\chi \to 0$ implies $p \ll q$, specifying a high barrier. When $\xi = qa \to \infty$ either $q \to \infty$ or $a \to \infty$; the former is only consistent with $\chi \to 0$, so in the limit of $\chi \to \infty$ the latter implies a long-range barrier. On the other hand, $\xi \to 0$, is only consistent with $a \to 0$, corresponding to a short-range barrier. Note that counterintuitively, the no barrier configuration corresponds to $\chi = -i$ and not $\chi = 0$. While it is true that $a = 0$ implies $\xi = 0$, this does not necessarily imply no scattering (c.f. delta-function barrier).

2.2.1   Wigner Time Delay

Consider the wavepacket after transmission,

$$\Psi_{III} = \int \, \mathrm{d}p \, |T(p)| \, \exp\left[i \left(\varphi(p) + p\,x - E(p)t\right)\right], \tag{2.16}$$

where $T = |T|e^{i\varphi}$. Note that the change of the transmission phase φ with respect to the momentum determines how the scattering affects the wavepacket since the latter is a superposition of waves of varying frequency. The maximum of this amplitude occurs when all p-component waves add constructively. This occurs at a stationary point of the phase in Eq. (2.16), that is when

$$x = p_0 \, t - \left[\frac{\partial \varphi}{\partial p}\right]_{p=p_0}. \tag{2.17}$$

In the absence of a potential barrier, the peak travels at the classical velocity p_0 (in atomic units). Equation (2.17) shows that the barrier causes a delay of the peak in reaching a given position x, a delay which is given the by the energy derivative of the transmission phase. This measure of the delay experienced by the peak forms the basis of the Wigner time concept. For the box potential, the time delay of the peak after crossing a barrier of length a is given by

$$\tau = \frac{1}{p_0} \left[\frac{\partial \varphi}{\partial p}\right]_{p=p_0} + \frac{a}{p_0}. \tag{2.18}$$

Explicitly, the time delay for a barrier of height χ and length ξ is given by the expression:

$$\tau = \frac{\xi \, \chi}{p_0} \frac{\frac{1}{2\xi}\left(\chi + \frac{1}{\chi}\right)^2 \tanh(\xi) + \frac{(1-\chi^2)}{2} \mathrm{sech}^2(\xi)}{1 + \frac{1}{4}\left(\chi - \frac{1}{\chi}\right)^2 \tanh^2(\xi)}. \tag{2.19}$$

This distribution is shown in Fig. 2.2. For longer barriers, $\xi \gg 1$, the tunnelling time τ becomes independent of the barrier length a and dependent only on the barrier height V_0,

$$\lim_{\xi \gg 1} \tau \approx \frac{a}{p_0} \frac{2}{\xi} = \frac{2\chi}{p_0} = \frac{2}{p_0} \frac{1}{\sqrt{2(V_0 - E)}}. \tag{2.20}$$

Interestingly, and perhaps counterintuitively, as ξ goes to infinity, τ vanishes: the longer the barrier, the less time it takes the peak to cross it. This is known as the Hartman effect [56, 57]; this effect is not so pathological as it seems, and is merely an interference effect. An interesting discussion of the relativistic implications of any superluminal information transmission may be found in [58].

What causes this delay of the peak? To answer "the barrier" merely shifts the question to "what happens at the barrier?" Wave mechanics tells us that when a wave is
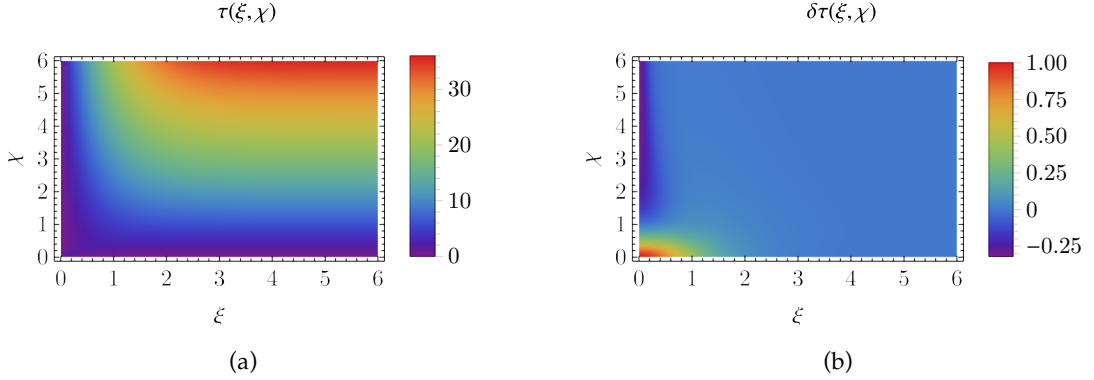
Figure 2.2: (a) Wigner time $\tau(\chi, \xi)$ for the box potential, as given by Eq. (2.19), for a given wave component $p_0 = 1/3$ a.u.. Note that for large ξ, i.e. long barriers, this time is constant for all barrier heights χ. Hence, the dominant parameter in tunnelling time is the barrier length ξ. (b) Normalized difference of time delay at each barrier, $\delta\tau = (\tau_{exit} - \tau_{entry})/(\tau_{exit} + \tau_{entry})$, showing that for long barriers ($\xi \gg 1$), the contribution to the total time delay is equally caused by both reflection across both barriers.

incident on a potential some portion is reflected and the rest is transmitted. This happens at every potential boundary; it follows that the transmitted waves interfere with the reflections from the boundaries and their superposition ultimately shapes the wave, shifting the peak.

The longer the barrier, the more suppressed reflected wave components become and hence less interference with transmitted wave components. This also explains why for very long barriers, the Wigner time becomes essentially independent of the length of the barrier. While this may seem unreasonable, it is important to note that the Wigner time measures changes in phase and so amplitudes, which determine the probabilities of tunnelling, play no direct role in this measure.

While this principle underlies much of the results of this section, one can go further and investigate what happen to the Wigner time if reflections from the boundary are suppressed.

2.2.2   Reflections and Time Delay

In the above problem there are two reflections: the reflection of the incoming wave from the barrier surface at $x = 0$, of the form $e^{-i p x}$, and the reflection of the tunnelled wavepacket from the barrier edge at $x = a$, of the form $e^{+q x}$. As can be deduced from Eq. (2.12) the reflection co-efficient C_1 in, the reflection at $x = a$ will decrease with increasing barrier length, $\xi \gg 1$, since $\lim_{\xi \to \infty} C_1 \propto e^{-\xi}$. As shown above, for $\xi \to \infty$ the time delay τ vanishes, suggesting the origin of the tunnelling time is related to the reflection of the tunnelling wavepacket.

Equations (2.19) and (2.20) yield the total time delay after tunnelling i.e. after re-

flection from both barrier boundaries. One can deduce the time delay caused by re-flection at the entry by applying the Wigner delay formula at $x = 0$. For $\xi \gg 1$, $R \approx -(1 + i\chi)/(1 - i\chi)$ and

$$\tau_{entry} = \frac{-i}{p_0} \frac{\partial}{\partial p} \ln\left(\frac{\psi_I(x)}{|\psi_I(x)|}\right)\bigg|_{x=0} \tag{2.21}$$

$$\approx \frac{a}{p_0} \frac{1}{\xi} = \frac{1}{2} \lim_{\xi \gg 1} \tau. \tag{2.22}$$

This is half of the total Wigner tunnelling time. The other half of the tunnelling time for large barriers is ostensibly due to the time delay from the interface when leaving the barrier. The Wigner delay at the exit can then defined as the difference between these two times:

$$\tau_{exit} = \tau - \tau_{entry}. \tag{2.23}$$

It is relatively easy to calculate the normalised time delay difference,

$$\delta\tau = \frac{\tau_{exit} - \tau_{entry}}{\tau_{exit} + \tau_{entry}} = \frac{\tau_{exit} - \tau_{entry}}{\tau}, \tag{2.24}$$

which is plotted in Fig. 2.2(b). It shows that in the regime where the barrier is long ($\xi \gg 1$), the tunnelling time is made up in equal parts by reflections from the entry and interfaces[4]. This forms a central point in this thesis: the reflections of waves incident on a scattering centre or potential work to slow down the peak of the wavefunction. This can also be applied to pure tunnelling phenomena, rather than just scattering. These are explored in the following chapters, where the principles developed here are applied to increasingly more sophisticated models of ionisation whilst at the same maintaining an analytic understanding of the underlying physics.

---

[4]It should be noted that in regions where that is not the case e.g. $\chi \to \infty$ or $\xi \to 0$, it is unlikely the Wigner time can provide a good measure of time delay as the distortion of the travelling wavepacket is likely significant

Chapter 3

Strong Field Ionization Theory

Having discussed the concepts associated with time delay in quantum mechanics, it is now possible to apply these to ionization problems. In this chapter, the relevant aspects of strong field ionization theory are laid out, which will pave the way for the results of the following chapters. The Hamiltonian for an electron-nucleus-laser system may be written as

$$H = H_{\text{atom}}(\mathbf{r}) + H_{\text{laser}}(\mathbf{r}, t). \tag{3.1}$$

For the eigenstate of the atomic Hamiltonian, $|\psi_a\rangle$, the probabilities of ionization of the bound state are dependent on the overlap $\langle \psi(t) | \psi_a(t) \rangle$, where $|\psi(t)\rangle$ is the full solution to the above Hamiltonian. In time evolution, or Green's function, language, the amplitude of ionization as measured at a detector is then

$$m = \lim_{\substack{t \to \infty \\ t_i \to -\infty}} \langle \psi(t) \,|\, U(t, t_i) \,|\, \psi_a(t_i) \rangle, \tag{3.2}$$

where $U(t, t_i)$ is the time evolution operator for the full Hamiltonian (3.1). One of the main aims of this chapter is to find an expression for $U(t, t')$ that accurately describes ionization, simple enough to be tractable but whose physical properties can be discussed without ambiguity. As with most three body problems, it is not possible to write down a general solution. To this end judicious approximations must be introduced which are standard in strong field studies.

3.1 Electromagnetic Interaction Theory

The first approximation is a conceptual one: it is assumed that in an atom only the outermost least energetically bound electron is susceptible to ionization. This is known as the *single active electron* approximation. In this study, it is trivially satisfied since for simplicity only atomic hydrogen is considered.

Secondly, only interactions with the most intense high-energy lasers require a relativistic treatment since in these cases the ionized electron is accelerated to relativistic speeds. Thus, one may begin by considering the non-relativistic Hamiltonian of an electron in an electromagnetic field,

$$H_{EM} = \frac{-\nabla^2}{2} - \frac{i}{2}\left(\mathbf{A}\cdot\nabla + \nabla\cdot\mathbf{A}\right) + \frac{\mathbf{A}^2}{2} - \varphi \tag{3.3}$$

for a laser with electric field $\boldsymbol{\mathcal{E}}(\mathbf{r},t) = -\nabla\varphi - \partial_t\mathbf{A}$ and magnetic field $\mathbf{B}(\mathbf{r},t) = \nabla\times\mathbf{A}$. Here, φ and $\mathbf{A}$ are the respective electromagnetic scalar and vector potentials and $\mathbf{r}$, t denote the radial vector pointing from the origin to the electron and time, respectively.

The Dipole Approximation

For the cases where the wavelength λ of an electric field $\boldsymbol{\mathcal{E}}(\mathbf{r},t)$ is large compared to the lengthscale of the atomic system system in question, as is the case throughout this work, spatial variations in the electric field can be neglected. That is, the electric field can be approximated

$$\boldsymbol{\mathcal{E}}(\mathbf{r},t) \approx \boldsymbol{\mathcal{E}}(t) = -\frac{d\mathbf{A}(t)}{dt}. \tag{3.4}$$

It follows that the magnetic field $\mathbf{B} = \nabla\times\mathbf{A}(t) = \mathbf{0}$ also vanishes. This is termed the *dipole approximation*. The dipole approximation is valid in non-relativistic systems such as the one considered here.

The Length Gauge

The Schrödinger equation is invariant under gauge transformations of the type

$$\psi(\mathbf{r},t) \to \bar{\psi} = e^{i\,f(\mathbf{r},t)}\,\psi(\mathbf{r},t), \tag{3.5}$$

provided the EM potentials in Equation (3.3) transform accordingly[1]. A common choice is $f(\mathbf{r},t) = -\mathbf{A}(t)\cdot\mathbf{r}$. With this transformation, the Schrödinger equation reads simply

$$i\frac{\partial}{\partial t}\psi(\mathbf{r},t) = \left(-\frac{\nabla^2}{2} + \boldsymbol{\mathcal{E}}\cdot\mathbf{r}\right)\psi(\mathbf{r},t), \tag{3.6}$$

where the interaction Hamiltonian $H_f = \boldsymbol{\mathcal{E}}(t)\cdot\mathbf{r}$ couples the electric field $\boldsymbol{\mathcal{E}}(t)$ to the radial vector, hence the name *length gauge*. Another commonly used gauge in strong field physics is the velocity gauge, but as will be reasoned later this latter gauge poses some disadvantages. The curious reader is referred [59] for an overview of EM gauge theory in strong fields.

---

[1]For a gauge transformation of this type $\mathbf{A}(\mathbf{r},t) \to \bar{\mathbf{A}}(\mathbf{r},t) = \mathbf{A}(\mathbf{r},t) + \nabla f(\mathbf{r},t)$ and $\varphi(\mathbf{r},t) \to \bar{\varphi}(\mathbf{r},t) = \varphi(\mathbf{r},t) - \frac{\partial}{\partial t}f(\mathbf{r},t)$. In the length gauge, $\bar{\mathbf{A}} = \mathbf{0}$ and $\bar{\varphi} = \left(\frac{\partial\mathbf{A}}{\partial t}\right)\cdot\mathbf{r} = -\boldsymbol{\mathcal{E}}(t)\cdot\mathbf{r}$.

The Volkov States

The Schrödinger equation (3.6) can surprisingly be solved exactly for *any* electric field $\mathcal{E}(t)$ [60]. Its solutions are known as the Gordon-Volkov states [61]:

$$|\Psi_{\mathbf{p}}(t)\rangle = |\mathcal{P}(t)\rangle \, e^{-i\,\mathcal{S}(t)}, \tag{3.7}$$

where $|\mathcal{P}(t)\rangle = |\mathbf{p} + \mathbf{A}(t)\rangle$ is a d-dimensional plane wave state, $\langle r|\mathbf{p}\rangle = e^{i\mathbf{p}\cdot\mathbf{r}}\,(2\pi)^{\frac{-d}{2}}$, modulated by the phase

$$\mathcal{S}(t) = \frac{1}{2}\int^t \mathrm{d}\tau\,\mathcal{P}(\tau)^2 = \frac{1}{2}\int^t \mathrm{d}\tau\,(\mathbf{p} + \mathbf{A}(\tau))^2. \tag{3.8}$$

The lower limit is usually unspecified since it contributes only a trivial phase to wavefunctions. These solutions describe the propagation of an electron in the electric field $\mathcal{E}(t)$. The relativistic generalisation was carried out by Volkov [62] so often, and hereafter, they are simply described as *Volkov states*. Since these are eigenstates of the Hamiltonian $H = -\nabla^2/2 + H_f$, the time evolution operator for an electron in the laser field can be expressed

$$U_f(t, t_i) = \int_{-\infty}^{\infty} \mathrm{d}p\,\,|\Psi_{\mathbf{p}}(t)\rangle\,\langle\Psi_{\mathbf{p}}(t_i)|, \tag{3.9}$$

which will be of use later.

3.2 The Strong Field Approximation

Weaving all these concepts together, the length gauge Hamiltonian for an electron in the combined atomic and laser field in the dipole limit, reads simply

$$H = -\frac{\nabla^2}{2} + \mathcal{E} \cdot \mathbf{r} + V(\mathbf{r}) \tag{3.10}$$

where $V(\mathbf{r})$ is the atomic potential. So far, no choice has been made for either the laser field or the atomic potential. The dynamics of the electron in the combined fields are described by the application of the Hamiltonian (3.10) to the time-dependent Schrödinger equation (TDSE):

$$i\frac{\partial\psi}{\partial t} = \left(-\frac{\nabla^2}{2} + \mathcal{E} \cdot \mathbf{r} + V(\mathbf{r})\right)\psi. \tag{3.11}$$

With modern computational tools, this equation can be numerically integrated for a range of atomic and laser potentials in an essentially exact manner. This allows for

accurate analysis and prediction of experimental results. However, the downside to such numerical integration is that the competing physical effects are not readily identifiable and only the resultant physical observables (via the solution $\psi(t)$) are accessible. In what follows, a standard approximation technique, known as the Strong Field Approximation [9, 63], is introduced with the aid of time evolution operators in order to produce a solution that is amenable to physical interpretation.

3.2.1   The Interaction Picture

Consider the Schrödinger equation for a general state $|\psi\rangle$ in the Schrödinger picture:

$$i\frac{\partial}{\partial t}|\psi(t)\rangle = H(t)|\psi(t)\rangle.$$

(3.12)

For a class of problems, the full Hamiltonian can be split into an explicitly time independent "free" part that is readily solveable and a time dependent interacting part whose solution is sought:

$$H(\mathbf{r}, \mathbf{p}, t) = H_0(\mathbf{r}, \mathbf{p}) + H_{\text{int}}(\mathbf{r}, \mathbf{p}, t).$$

(3.13)

The idea is to split all operators and states in the Schrödinger picture into free and interacting states, with the time dependence (usually) being present in only the interacting states, in what is known as the *interaction picture*. The formal solution to Equation (3.12) is given by

$$|\psi(t)\rangle = U(t, t_i)|\psi(t_i)\rangle$$

(3.14)

where $U(t, t_i)$ is the time evolution operator, which unitarily evolves the wavefunction $|\psi\rangle$ from some initial time t_i to some later time t. In the interaction picture the time evolution operator can be expressed as

$$U(t, t_i) = U_0(t, t_i) - i\int_{t_i}^{t} dt_1\, U(t, t_1)\, H_{\text{int}}(t_1)\, U_0(t_1, t_i),$$

(3.15)

where $U_0(t, t_i)$ is the time evolution operator for the unperturbed Hamiltonian H_0. Equation (3.15) is known as the Dyson equation[2] and it is a transcendental equation in $U(t, t_i)$. Successive iterations of the Dyson equation yield the formal solution as an infinite sum, known as a Dyson series:

$$U(t, t_i) = \sum_{n=0}^{\infty} \bar{U}^{(n)}(t, t_i),$$

(3.16)

with each term given by

$$\bar{U}^{(n)}(t, t_i) = (-i)^n \left(\prod_{k=1}^{n} \int_{t_i}^{t_{k-1}} dt_k\, U_0(t_{k-1}, t_k)\, H_{\text{int}}(t_k)\right) U_0(t_n, t_i),$$

(3.17)

---

[2]An intuitive derivation of the Dyson equation may be found Appendix B.

where the integrals are understood to be time ordered ($t > t_1 > ... > t_n$) and $t_0 \equiv t$. It should be pointed out that the Dyson series is analogous to the Born approximation method of usual scattering theory (see e.g. [55, 60, 64]).

Weak Field Perturbation Theory

It is instructive to consider a simple example. Taking the free Hamiltonian to describe the atom

$$H_0 \longrightarrow H_a = -\frac{\nabla^2}{2} + V(\mathbf{r}) \tag{3.18}$$

and the interaction Hamiltonian to describe the interaction with the laser field

$$H_{\text{int}} \longrightarrow H_l = \boldsymbol{\mathcal{E}}(t) \cdot \mathbf{r}, \tag{3.19}$$

with respective evolution operators $U_a(t, t_i)$ and $U_f(t, t_i)$, defines the evolution operator

$$U(t, t_i) = U_a(t, t_i) - i \int_{t_i}^{t} \mathrm{d}t_1 \, U(t, t_1) \, H_l(t_1) \, U_a(t_1, t_i). \tag{3.20}$$

With these operators, Eq. (3.17) can be interpreted as follows (from right to left): initially at time t_i the electron is in a bound state $|\psi(t_i)\rangle$ and evolves according to the atomic evolution operator $U_a(t_n, t_i)$ up to time t_n where it interacts with the laser field via $H_{\text{int}}(t_n) = H_l(t_n)$. After this interaction, the electron again evolves under the dynamics of an atomic evolution operator $U_a(t_{n-1}, t_n)$ until time t_{n-1}, when another interaction takes place. If the infinite series (3.16) is truncated at $n = N$, this cascade continues until $k = N$ meaning the electron has experienced N interactions with the laser field. That is, this expression can be understood as an N-photon process of emission and/or absorption.

Notwithstanding the formal solution, Eq. (3.17), the Dyson series are typically asymptotic series, with dependence on some smallness parameter and they must be truncated. This type of truncated perturbation series in the interaction Hamiltonian H_{int} converges when free evolution operator $U_0(t, t_i)$ is similar to the full evolution operator $U(t, t_i)$, i.e. for weak fields [60].

The Strong Field Approximation

However, when the the laser field strength is comparable with the atomic potential such a truncated series is no longer a suitable description of the underlying physics. In particular, there is a strong likelihood of the electron escaping the atom and hence no longer obeying the unitary evolution given by the free-field operator U_0. In this case, the ionized electron is propagated in the laser field away from the atomic core; this propagation

is described by an evolution operator of the form (3.15) but now with the interaction being the atomic potential

$$H_0 \longrightarrow H_f = -\frac{\nabla^2}{2} + \boldsymbol{\mathcal{E}}(t) \cdot \mathbf{r}, \tag{3.21}$$

and the "free field" being the evolution in the field,

$$H_{\text{int}} \longrightarrow H_V = V(\mathbf{r}). \tag{3.22}$$

Recall that the Hamiltonian (3.21) has an evolution operator $U_f(t, t') = \int |\psi_{\mathbf{p}}(t)\rangle \langle \psi_{\mathbf{p}}(t')|$ expressible in terms of the Volkov states. The evolution operator for this new interaction will then obey the Dyson equation

$$U_{\text{SFA}}(t, t_i) = U_f(t, t_i) - i \int_{t_i}^{t} dt_1 \, U_{\text{SFA}}(t, t_1) \, V(\mathbf{r}) \, U_f(t_1, t_i). \tag{3.23}$$

The *Strong Field Approximation* (SFA) assumes that after ionization, the laser field carries the electron far away from the nucleus and thus dominates the electron dynamics succh that any further interactions with the nucleus can be treated perturbatively. Formally, this corresponds to substituting the full time evolution operator $U(t, t_i) \longrightarrow U_{SFA}(t, t_i)$ in the right-hand side. of Eq. (3.20),

$$U(t, t_i) = U_a(t, t_i) - i \int_{t_i}^{t} dt_1 \, U_{SFA}(t, t_1) \, H_l(t_1) \, U_a(t_1, t_i), \tag{3.24}$$

and moreover, replacing the final state $|\psi(t)\rangle$ in Eq. (3.2) with the Volkov state $|\psi_{\mathbf{p}}(t)\rangle$ (i.e. the solution of the electron propagating in the laser). As before, a formal solution to this time evolution operator is given by

$$U(t, t_i) = \sum_{n=0}^{\infty} \tilde{U}^{(n)}(t, t_i), \tag{3.25}$$

with each term

$$\tilde{U}^{(n)}(t, t_i) = (-i)^n \left(\prod_{k=1}^{n} \int_{t_i}^{t_k-1} dt_k \, V(\mathbf{r}) \, U_f(t_{k-1}, t_k) \right) H_n(t_n) \, U_a(t_n, t_i), \tag{3.26}$$

where $H_n(t_n) = H_l(t_n)$ for $n \geq 1$, and unity otherwise. More explicitly, the first few orders are

$$\tilde{U}^{(0)}(t, t_i) = U_a(t, t_i), \tag{3.27}$$

$$\tilde{U}^{(1)}(t, t_i) = -i \int_{t_i}^{t} \mathrm{d}t_1 \, U_f(t, t_1) \, H_l(t_1) \, U_a(t_1, t_i), \tag{3.28}$$

$$\tilde{U}^{(2)}(t, t_i) = -\int_{t_i}^{t} \mathrm{d}t_1 \int_{t_1}^{t} \mathrm{d}t_2 \, U_f(t, t_1) \, V \, U_f(t_1, t_2) \, H_l(t_2) \, U_a(t_2, t_i), \tag{3.29}$$

and so forth to higher orders. Analogously to Eq (3.17), Eq. (3.26) may be interpreted as the evolution of a bound state at initial time t_i, which interacts with the laser field at time t_n through $H_l(t_n)$ and is ionized and subsequently propagated in the laser field by $U_f(t_{n-1}, t_n)$ until a re-scattering with the atomic potential $V(\mathbf{r})$ occurs. For a given n, the wavefunction $|\tilde{\psi}^{(n)}(t)\rangle = \tilde{U}^{(n)}(t, t_i) |\psi_a(t_i)\rangle$ describes the ionization of an electron with $n-1$ re-scattering events with the atomic potential before being carried off by the laser field.

The SFA Wavefunction and Amplitudes

The complete wavefunction for the electron is then given by applying the unitary evolution operator in the SFA to the initial atomic state, $|\psi(t)\rangle = U(t, t_i) |\psi_a(t_i)\rangle$. This can be expressed as $|\psi(t)\rangle = |\psi_a(t)\rangle + |\psi_i(t)\rangle + |\psi_r(t)\rangle + \mathcal{O}(V^2)$, where

$$|\psi_i(t)\rangle = \tilde{U}^{(1)}(t, t_i) |\psi_a(t_i)\rangle = -i \int_{t_i}^{t} \mathrm{d}t_1 \int_{-\infty}^{\infty} \mathrm{d}\mathbf{p} \, |\Psi_{\mathbf{p}}(t)\rangle \langle \Psi_{\mathbf{p}}(t_1)|H_l(t_1)|\psi_a(t_1)\rangle \tag{3.30}$$

is the wavefunction describing direct ionization, and $|\psi_r(t)\rangle = \tilde{U}^{(2)}(t, t_i) |\psi_a(t_i)\rangle$ describes an ionization with one scattering event with the atomic core. Higher orders in V describe ionization with the corresponding number of rescattering events. Equation (3.30), corresponding to direct ionization, forms the basis of this study since it is the dominant term in the series, although rescattering is eventually considered in Chapter 6.

In the SFA, the asymptotic amplitude for ionization with $n-1$ recollision processes is

$$m_n(\mathbf{p}) = \lim_{t \to \infty} \langle \psi_{\mathbf{p}}(t) \,|\, \psi(t) \rangle = \lim_{t \to \infty} \langle \psi_{\mathbf{p}}(t) \,|\, \tilde{U}^{(n)}(t, t_i) \,|\, \psi_a(t_i) \rangle \tag{3.31}$$

where the SFA dictates the replacement of the final wavefunction with the Volkov state $|\psi_{\mathbf{p}}(t)\rangle$. The amplitudes $m_1, m_2, \dots$, can then be interpreted as the amplitudes of ioni-

sation with no recollision, probability of ionisation after one recollision, *et cetera* [3], and their coherent superposition and integration over momentum would yield the experimentally measurable photoelectron momentum distributions. Unlike most studies of time delay, this work will mostly concern the the wavefunction at intermediate times, $|\psi_i(t)\rangle$, as opposed to the well understood probability for the same process at large times, $|m_1(\mathbf{p})|^2$, since the aim here is to deconstruct electron dynamics *during* the tunnelling process.

The SFA is a staple of strong field ionization studies partly because it lends itself to the simple series interpretation outlined above, in contrast to other numerical techniques. It is not, however, without its flaws. In particular, it is not *a priori* gauge invariant, since the choice of division of the Hamiltonian into free and interacting parts may lead to inconsistencies. It has been reported [65] that for Coulomb potentials, the length gauge (with the dipole approximation) is able to reproduce TDSE results to exponential accuracy, unlike the velocity gauge. Faisal [66] showed the equivalency of the two gauges for a given choice of the division of the Hamiltonian. It has also been shown for short-range potentials, the SFA takes the same form in the length and velocity gauges. Exactly to bypass these (and other) difficulties, the choice was made in this work to use the standard representation of the SFA in the length gauge and moreover to work with the delta function potential.

3.3   The Zero Range Potential

The potential of choice for this study is the the Dirac delta-function, known also as the zero range potential (ZRP), reads in one dimension

$$V(x) = \lambda\,\delta(x), \tag{3.32}$$

where $\lambda < 0$ for an attractive potential. Much like the divergent Coulomb potential, this is a pathological potential, used to model an underlying ignorance of the physics at the atomic core.

The ZRP is used for two good reasons. Firstly, it is short range, so the interaction is not present over all space; mathematically, this simplifies a lot of integrals and keeps calculations tractable. Secondly, since the Coulomb potential stretches over all space, it becomes difficult to isolate contributions from e.g. the laser field. With the ZRP, the interaction is not drawn out so one can in principle separate the laser and atom contributions to the dynamics.

The time independent Schrödinger equation for this potential is given by

$$\left(-\frac{1}{2}\frac{\mathrm{d}^2}{\mathrm{d}x^2} + \lambda\,\delta(x)\right)\psi(x) = E\,\psi(x) \tag{3.33}$$

---

[3]Note that while the true final state $|\psi(t)\rangle$ is orthogonal to the bound state $|\psi_a\rangle$, this is not the case for the Volkov states so $m_0 \neq 0$. This is a consequence of the non-linear perturbation theory employed but has no bearing on the interpretation of the solutions since on is usually interested only in probabilities of ionization (i.e. orders $n \geq 1$).

For a given energy $E = k^2/2$, the potential permits exactly one bound state ($E < 0$) and a continuous range of free, or scattering, states ($E > 0$). The wavefunction is in both cases separated piecewise into $x > 0$ and $x < 0$ components, with the coefficients dictated by wavefunction continuity across the singularity at the origin (see e.g. [67]).

The Bound State

For the bound state $E < 0$, with $k = \sqrt{-2|E|} \equiv i\kappa$, the wavefunction is given by

$$\psi_0(x) = \sqrt{\kappa}\, e^{-\kappa\,|x|}, \tag{3.34}$$

with the condition that $\lambda = -\kappa$ (i.e. an attractive potential). This wavefunction is continuous everywhere but its derivative is discontinuous at the origin. For strong field ionization, the energy E is taken to be the binding energy I_p of the atom, such that $I_p = \kappa^2/2$.

The Scattering States

For energies $E > 0$, with $k = \sqrt{2E}$, the scattering wavefunction takes the form

$$\psi_{sc}(x) = \begin{cases} e^{ikx} + Be^{-ikx} & x < 0 \\ \\ Ce^{ikx} & x > 0. \end{cases} \tag{3.35}$$

where

$$B = \frac{i/k}{1 - i/k}, \qquad \text{and} \qquad C = \frac{1}{1 - i/k}. \tag{3.36}$$

To model scattering by the potential it should be noted that in definition (3.35) the incoming wave amplitude has been set to unity and only outgoing wave are considered, without loss of generality.

In this work, the bound state wavefunction will be used extensively throughout as the model for the single active electron. However, the scattering states will come in useful for calculations involving higher order rescattering events, such as in the Low Frequency Approximation of Chapter 6.

With the theoretical toolbox developed, one may now proceed in applying the SFA with the zero-range potential to the study of ionization. The first case considered is an adiabatic laser field which allows for the connection with the Wigner time delay to be made fully analytically.

Chapter 4

Ionization in a Static Laser Field

"Il apparut que, entre deux vérités du domaine réel, le chemin le plus facile et le plus court passe bien souvent par le domaine complexe."

"*It came to appear that, between two truths of the real domain, the easiest and shortest path quite often passes through the complex domain.*"

Paul Painlevé

Having developed some notion of time delay and of ionization in the previous chapters, applications to physical models may be explored. The analysis of the Wigner time delay in Chapter 2 concerned a type of scattering event which is, at a closer look, a different process to that of ionization: the ionization process begins from *within* the barrier in the first place. Thus, a wavefunction is not incident on a potential but rather a bound state continually "leaks out" of the potential barrier.

Nonetheless, the two processes are not wholly distinct. The wavefunction dynamics are still dictated by the characteristics of the potential barrier. In both cases if one observes a time delay for the scattering scenario, one would expect an analogous phenomenon for the ionization. In a realistic description of ionization, the barrier varies significantly in space and time. As a consequence, the ionised electron wavefunction will longer be simply separable into transmitted or reflected components, as it was in Chapter 2. In order to explore more realistic models of ionization, time dependence of the electric field is eschewed in this chapter.

Ionization by a static field is considered for two simple models: the time independent Schrödinger equation (TISE) and an SFA time evolved wavefunction as described in Chapter 3. From the analysis of the former, a method of separating transmission and reflection components for the latter can be derived. This clears the path for applying
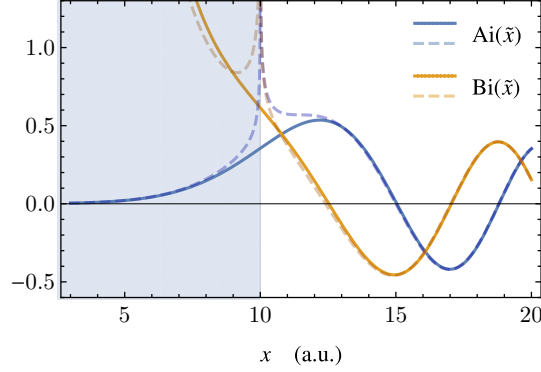
Figure 4.1: The solution to the electron in a constant field problem is given by a superposition of Airy functions of the first and second kind, $\text{Ai}(\tilde{x})$ and $\text{Bi}(\tilde{x})$, plotted in blue and orange respectively. These functions have very accurate asympotic expansions, shown dashed, which can be derived by considering the saddle points of the Airy integrals (4.13)-(4.14). Under the barrier, $x < 10$ (shaded blue), these expansions show that the wavefunction components $\text{Ai}(\tilde{x})$ and $\text{Bi}(\tilde{x})$ respectively correspond to the reflected and transmitted components of the wavefunction.

this method to a fully time dependent field in later chapters.

4.1   Adiabatic Ionization in Constant Field

Begin by considering a bound electron of energy $-I_p$ in a one dimensionsl zero range potential, ionized by a constant electric field $\mathcal{E}(t) \approx -\mathcal{E}_0$ (i.e. a field which varies only adiabatically). The continuum eigenstate of the electron in this field is given by the solution to the time-independent Schrödinger equation:

$$-\frac{1}{2}\frac{\mathrm{d}^2\psi}{\mathrm{d}x^2} + (I_p - \mathcal{E}_0\,x)\,\psi(x) = 0. \tag{4.1}$$

By performing a change of variables

$$\tilde{x} = 2^{1/3}\,\mathcal{E}_0^{-2/3}\,(I_p - \mathcal{E}_0\,x), \tag{4.2}$$

this equation can be cast into a more recognisable form, namely $\psi''(\tilde{x}) - \tilde{x}\,\psi(\tilde{x}) = 0$. This is the Airy equation. A general solution is a superposition of the Airy functions of the first and second kind $\psi(x) = c_1\text{Ai}(\tilde{x}) + c_2\text{Bi}(\tilde{x})$. These solutions are sketched out in Fig. 4.1.

The wavefunction is required to be a travelling wave to the right in the continuum after ionization[1], forcing $c_1 = -i\,c_2$. The general solution is then

---

[1]The phase difference between the two coefficients must be such the probability current, $j = i/2\,(\psi(x)\psi'(x)^* - \psi(x)^*\psi'(x))$, is maximal.

$$\psi(x) = T\left[\mathrm{Ai}(\tilde{x}) - i\,\mathrm{Bi}(\tilde{x})\right], \tag{4.3}$$

where T is a prefactor determined by matching the wavefunction to the bound-state solution of the atom, $\psi_0(x)$. The Wigner time is dependent only on derivatives of the phase, is unaffected by T, so we do not concern ourselves with this term. It can be calculated straightforwardly

$$\tau_W(x) = i\frac{\partial}{\partial I_p}\ln\frac{\psi}{|\psi|} = \frac{2^{\frac{1}{3}}}{\pi\mathcal{E}_0^{\frac{2}{3}}}\frac{1}{\mathrm{Ai}(\tilde{x})^2 + \mathrm{Bi}(\tilde{x})^2}. \tag{4.4}$$

This is interpreted as the trajectory of the peak of a tunnelled electron wavepacket under a constant electric field, and may be used as a benchmark for results in later chapters. Likewise, it is simple to estimate the scaling of the Wigner time delay at the tunnel exit $x_e = I_p/\mathcal{E}_0$

$$\tau_W(x_e) = \frac{3^{4/3}\,\Gamma\left(\frac{2}{3}\right)^2}{2^{5/3}\pi}\mathcal{E}_0^{-2/3}. \tag{4.5}$$

Additionally, the concept of the Wigner electron group velocity $v_W(x) = \left(\frac{\partial \tau_W(x)}{\partial x}\right)^{-1}$ is defined, which plays an analogue role to momentum for the peak of the wavefunction. At the classical tunnel exit, $x_e = I_p/\mathcal{E}_0$, it is found to be

$$v_W(x_e) = \frac{2\left(\frac{2}{3}\right)^{2/3}\sqrt{\pi}\,\Gamma\left(\frac{7}{6}\right)}{\Gamma\left(\frac{2}{3}\right)^2}\mathcal{E}_0^{1/3}. \tag{4.6}$$

These will be useful yardsticks for the time dependent case in Chapter 5, where we find good agreement. The above results are found to be consistent with the estimate of the scaling of the electron momentum $p_e \sim \mathcal{E}_0\,\tau_W$ in Ref. [68].

4.1.1 Contour Integral Solutions

Having obtained a solution for the electron in an adiabatic field and calculated its tunnelling time delay, it remains to analyse the origin of the latter. As discussed in Chapter 2, the cause is ostensibly the interference of transmitted (exponentially decaying) and reflected (exponentially growing) components of the wavefunction under the barrier.

How can these components be identified in the wavefunction? In order to identify these components, practical expressions for the two Airy functions are sought. Since the Airy equation is a Laplace linear equation, solutions may be expressed as complex contour integrals (see e.g. [69, §5.3]),

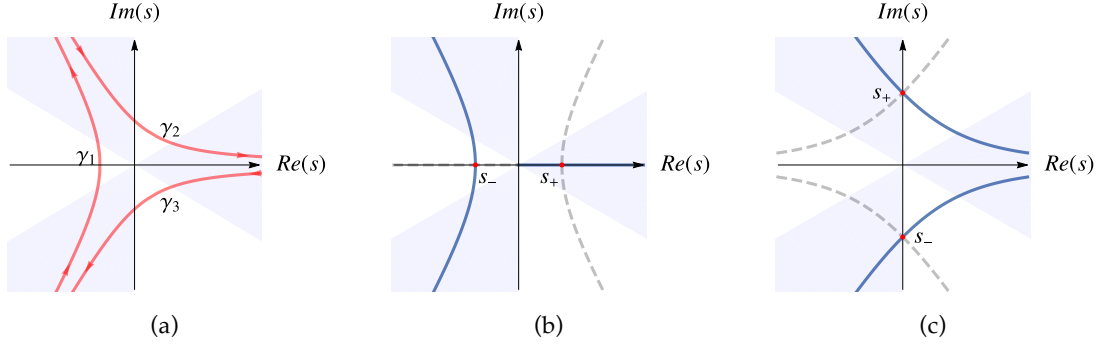$$\psi(x) = \int_\gamma e^{x\,s}P(s)\,\mathrm{d}s, \tag{4.7}$$

Figure 4.2:   The Airy integral $\int_\gamma ds \exp(\tilde{x} s - s^3/3)$ is defined on the complex s plane; it converges when the endpoints of its infinite contour, γ, lie in the shaded areas. The canonical contours defining the Airy function of the first (γ_1) and second ($\gamma_2 - \gamma_3$) kind are shown in **(a)**. Contributions to the Airy integral arise principally from portions of the contour near the saddle-points of the integrand function $\exp(\tilde{x} s - s^3/3)$. The configuration of the saddles $s_\pm = \pm\sqrt{\tilde{x}}$ (red dots) in the complex plane is shown for positions **(b)** inside the barrier ($\tilde{x} < 0$), and **(c)** outside the barrier ($\tilde{x} > 0$). Deforming the defining contours in (a) through the steepest descents contours (solid blue) in (b) and (c) provides asymptotic expansions for the Airy function, as in Eqs. (4.17) and (4.18). Dashed grey lines indicate the contours of steepest ascents.

where γ is a contour in the complex plane. The problem is then reduced to finding the function $P(s)$ and the contour γ which solve the differential equation. It follows from the Airy equation, $\psi''(\tilde{x}) - \tilde{x}\,\psi(\tilde{x}) = 0$, that

$$\int_\gamma (s^2 - x)\, e^{x s}\, P(s)\, \mathrm{d}s = 0. \tag{4.8}$$

Let $Q(s)$ be a function such that

$$\frac{\mathrm{d}}{\mathrm{d}s}\left(e^{x s}\, Q(s)\right) = (s^2 - x)\, e^{x s}\, P(s) \tag{4.9}$$

Comparing co-efficients in x one finds $-P(s) = Q(s)$ and $s^2 P(s) = Q'(s)$. This implies

$$Q(s) = e^{-\frac{s^3}{3}}. \tag{4.10}$$

Having obtained $P(s)$, only the contour γ remains to be determined. The Airy equation is satisfied provided γ obeys

$$\int_\gamma (s^2 - x)\, e^{x s}\, P(s)\, \mathrm{d}s = \int_\gamma \mathrm{d}s\, \frac{\mathrm{d}}{\mathrm{d}s}\left(e^{x s} Q(s)\right) = [e^{x s} Q(s)]_\gamma = \left[e^{x s - \frac{s^3}{3}}\right]_\gamma = 0. \tag{4.11}$$

That is, the equation is satisfied provided $\exp(x\,s - \frac{s^3}{3})$ takes the same value at the end-points of the contour γ. There is no finite contour satisfying this requirement and a closed contour yields only the trivial solution. However, a suitable *infinite* path may be found by examining under which conditions $\exp(x\,s - \frac{s^3}{3})$ vanishes.

In polar form, $s = r\,e^{i\theta}$, one has $|\exp(-s^3/3 + x\,s)| = \exp\left(-r^3/3\,\cos(3\theta)\right)|\exp(x\,s)|$ and so as $r \to \infty$ the integral vanishes wherever $\cos(3\theta) > 0$. This occurs when the end points lie at infinity in the regions

$$-\frac{\pi}{6} < \theta < \frac{\pi}{6}, \qquad \frac{\pi}{2} < \theta < \frac{5\pi}{6}, \qquad \text{and} \qquad \frac{7\pi}{6} < \theta < \frac{3\pi}{2}. \tag{4.12}$$

These regions are presented as shaded areas in Fig. 4.2 (a). Note also that non-trivial contour solutions must have start and endpoints in different regions since contributions in opposite directions from the same sector would cancel.

A variety of infinite contours satisfy these requirements but a second order ODE such as the Airy equation has only two linearly independent solutions. Let γ_1 be the contour originating at $\infty e^{i4\pi/3}$ and ending at $\infty e^{i\frac{2\pi}{3}}$, as indicated in Fig. 4.2 (a). Two other similar contours between the shaded areas can be chosen: γ_2 (starting from $\infty e^{i2\pi/3}$ and ending at $+\infty$) and γ_3 (starting at $+\infty$ and ending at $\infty e^{i4\pi/3}$). The canonical solutions to the Airy equation are then the Airy function of the first kind,

$$\text{Ai}(x) = \frac{1}{2\pi i} \int_{\gamma_1} \mathrm{d}s\ e^{x\,s - \frac{s^3}{3}}, \tag{4.13}$$

and the Airy function of the second kind, known affectionately as the "Bairy" function,

$$\text{Bi}(x) = \frac{1}{2\pi} \int_{\gamma_2 - \gamma_3} \mathrm{d}t\ e^{x\,s - \frac{s^3}{3}}. \tag{4.14}$$

The purpose of explicitly deriving the solutions to the Airy equation is to enlighten how one may identify which component of the wavefunction corresponds to transmissions and which to reflection. Merely by observation of Fig. 4.1, the Bi-component of the wavefunction decays exponentially as it approaches the tunnel exit, $x = x_e$, from the atomic core at $x = 0$, and hence can be seen to correspond to the transmission component; likewise, the exponentially growing Ai-component corresponds to wavefunction reflection.

4.1.2 Reflection, Transmission and Saddle Points

The above interpretation can be formally established by considering the integral representation of the Airy functions, Eqs (4.13) and (4.14), with the aid of Fig. 4.2 (a). The solution to the Schrödinger equation (4.1) may be considered as a contour integral

$$\psi(x) \propto \int_{\zeta} \mathrm{d}s\ \exp\left(\tilde{x}\,s - s^3/3\right) \tag{4.15}$$

where ζ is some combination of the defining paths γ_i of the Airy functions. Examining the integrand, one may notice it is a superposition of multiple frequency waves which for the most part cancel out, just as in the derivation of the Wigner time delay of Chapter 2. As before, the exception to this occurs when the phase difference between each s component wave is minimal (i.e. at an extremum of the phase $\tilde{x}\,s - s^3/3$). The majority of the contributions to the Airy integrals thus come from around the saddle points of the argument of integrand

$$s_\pm = \pm\sqrt{\tilde{x}}. \tag{4.16}$$

This idea forms the basis of a powerful technique, known as the saddle-point or steepest-descents method [69, 70] , used to accurately approximate highly oscillating integrals. The method is outlined in Appendix C and is grounded in the fact that the integration contours may be deformed, in this case the Airy contours γ_i, into contours that to go through these saddle-points and a mere expansion the integral around these saddle points is sufficient to achieve excellent approximations to such functions.

The saddle-points, and the respective paths of steepest descents, are illustrated in Figs. 4.2 (b) and (c); since these are dependent on $\tilde{x}$ the application of the saddle point method is different for the two cases of inside ($\tilde{x} < 0$) and outside ($\tilde{x} > 0$) the potential barrier. As shown in Fig. 4.2 (b), for $\tilde{x} < 0$ the contour γ_1 may be smoothly deformed into the path of steepest descents for the saddle point s_-, obtaining the asymptotic approximation

$$\mathrm{Ai}(\tilde{x}) = \frac{\exp\left(-\frac{2}{3}\tilde{x}^{\frac{3}{2}}\right)}{2\,\sqrt{\pi}\,\tilde{x}^{\frac{1}{4}}} + \mathcal{O}(\tilde{x}^{-\frac{3}{2}}). \tag{4.17}$$

Likewise, the contours γ_2 and $-\gamma_3$ may be deformed in both cases to go through the steepest descent path of the saddle point s_+ yielding the asymptotic form of the $\mathrm{Bi}(x)$-function under the potential barrier

$$\mathrm{Bi}(\tilde{x}) = \frac{\exp\left(+\frac{2}{3}\tilde{x}^{\frac{3}{2}}\right)}{\sqrt{\pi}\,\tilde{x}^{\frac{1}{4}}} + \mathcal{O}(\tilde{x}^{-\frac{3}{2}}). \tag{4.18}$$

Thus, from a tunnelling particle's perspective, one may identify the Airy function and its saddle-point s_- with the reflected part of the wavefunction, and the saddle-point s_+, or the Bairy function with the transmitted part of the wavefunction. The transmitted wave decays as it moves to the tunnel exit, while the reflected wave propagates from the exit decaying exponentially toward the atomic core, as shown in Fig. 4.1. Thus, using the contour ζ in equation (4.15) it is easy to identify and separate the transmitted and reflected wave components of the wavefunction by dividing the contour ζ into sections crossing each saddle point. This is equivalent to performing the saddle point approximation around each saddle.

This insight might seem trivial given the original solution (4.3) was already a superposition of two functions. One function is the reflected part and the other the transmitted part and the total wavefunction is naturally a superposition of these. This observation, however, presupposes that the wavefunction is separable into a sum of known functions; this is only really true when the spatial and temporal components of the wavefunction are themselves separable. This has been the case so far, but for the time evolution wavefunction introduced in Chapter 3 this is in general not the case. Temporal and spatial components are intermingled and the separation of the wavefunction into reflected and transmitted components is not straightforward.

Fortunately, the analysis of this Chapter has provided a clue on how to do exactly that: the key is to identify and analyse the saddle points of the wavefunction integral. In what follows, this proposition is applied to the SFA wavefunctin in a constant field. There, one is able to show analytically this correspondence of the saddle points to the under the barrier properties of the wavefunction. The concepts developed in the remainder of this chapter are then subsequently applied to the time-dependent field case, a physically more relevant scenario.

4.2 The Strong Field Approximation in the Constant Field

Consider the SFA wavefunction derived in Chapter 3, for the same electron in a zero range potential of binding energy $I_p = \kappa^2/2$,

$$\psi_i(x,t) = \int_{-\infty}^{\infty} dx' \int_{-\infty}^{\infty} dp \int_{t_i}^{t} dt' \left\langle x \,|\, \psi_p(t) \right\rangle \left\langle \psi_p(t') \,|\, H_i \,|\, \psi_0(t') \right\rangle, \qquad (4.19)$$

ionized by constant laser field $E(t) = -\mathcal{E}_0$. Due to the simplicity of the field, the corresponding vector potential $A(t) = -\int^t d\tau \, E(\tau) = \mathcal{E}_0 t$ and Volkov phase

$$S(t) = \frac{1}{2} \left(p^2 t + p\mathcal{E}_0 t^2 + \mathcal{E}_0^2 \frac{t^3}{3} \right) \qquad (4.20)$$

are simple polynomials in time. Letting $\mathcal{P}(t) \equiv p + A(t) = p + \mathcal{E}_0 \, t$, the wavefunction takes on the explicit form

$$\psi_i(x,t) = -i\frac{\sqrt{\kappa}\,\mathcal{E}_0}{2\pi} \int_{-\infty}^{\infty} dp \int_{-\infty}^{\infty} dq \int_{-\infty}^{t} dt' q \; e^{i\,(\mathcal{P}(t)\,x - \mathcal{P}(t')\,q + S(t') - S(t) + i\kappa|q| + I_p t')} \quad (4.21)$$

Since $S(t')$ is a cubic in t', one can already identify an Airy-type function in the t' integral by comparison to the integral definitions (4.13) and (4.14). However, to make this relation explicit and to cast the integral in a more tractable form, we may perform the following coordinate transforms:

$$t'' = t' + \frac{p}{\mathcal{E}_0} \qquad\qquad \text{and} \qquad\qquad p = P + \mathcal{E}_0\, t. \qquad (4.22)$$

In these variables the wavefunction integral takes the form

$$\psi_I(x,t) \propto \int_{-\infty}^{\infty} \mathrm{d}P\, e^{-\frac{i}{2\mathcal{E}_0}\left(P^3/3+\Pi(x)\,P\right)} \int_{-\infty}^{\infty} \mathrm{d}q\, q\, e^{-\kappa\,|q|} \int_{-\infty}^{P/\mathcal{E}_0} \mathrm{d}t''\, e^{i\,\frac{\mathcal{E}_0^2}{2}\left(t''^3/3+\Pi(q)\,t''\right)}$$

$$(4.23)$$

where $\Pi(y) \equiv 2(\mathcal{E}_0\, y - I_p)$. How may one calculate such an integral?

In the new variables, there are Airy-like arguments in the P and t'' integrals, indicating the wavefunction behaves roughly like a product of Airy functions. The only distinction is in the finitiness of the limits of the integrals; these types of functions rise in wave phenomena and are known as incomplete Airy functions [71]. The main issue in our case is that the P dependence of the limit (arising from the time dependence of the limit of the Dyson integral) prevents the separation of these integrals.

Recall the determining role of saddle points in the calculation of contour integrals. The saddle points of the two Airy arguments are given by $t''_\pm = \pm 1/\mathcal{E}_0\,\sqrt{\Pi(q)}$ and $P_\pm = \pm\sqrt{\Pi(x)}$ and, by examining the integration contours, the relevant saddle points for the steepest descents method applied to integral (4.23) are found to be $P_0 = -\sqrt{\Pi(x)}$ and

$$t''_0 = \frac{\sqrt{\Pi(q)}}{\mathcal{E}_0}. \qquad (4.24)$$

In order to be able to approximate the integral, consider the integration contour in t'' and divide it into two sections, as shown in Fig. 4.3: from negative infinity to the saddle point t''_0 and from this saddle point to the observation time $t = P/\mathcal{E}_0$,

$$\int_{-\infty}^{P/\mathcal{E}_0} \mathrm{d}t'' \quad\longrightarrow\quad \int_{-\infty}^{t''_0} \mathrm{d}t'' \quad + \quad \int_{t''_0}^{P/\mathcal{E}_0} \mathrm{d}t''. \qquad (4.25)$$

Each term in the integral is analysed as follows.

4.2.1   Integration up to saddle point

Consider the first portion of the integral,

$$\int_{-\infty}^{\infty} \mathrm{d}P\, e^{-\frac{i}{2\mathcal{E}_0}\left(\frac{P^3}{3}+\Pi(x)\,P\right)} \int_{-\infty}^{\infty} \mathrm{d}q\, q\, e^{-\kappa\,|q|} \int_{-\infty}^{t''_0} \mathrm{d}t''\, e^{i\,\frac{\mathcal{E}_0^2}{2}\left(t''^3/3+\Pi(q)\,t''\right)}. \qquad (4.26)$$
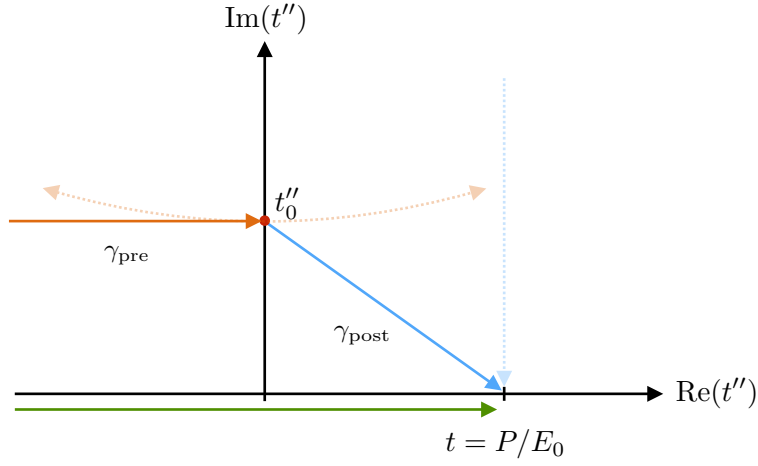
Figure 4.3: Overview of the integration in the complex t'' plane. The complete result for the full wavefunction is in green along the horizontal axis. The integration is split up into the path γ_{pre} up to the saddle point (orange) and the path γ_{post} down to the time t (blue). Dashed lines correspond to the approximations performed on these integrals, namely the steepest descent and Laplace methods.

Immediately it can be noted that these integrals are now tractable: the P integral is separable and moreover, the limit of the t'' integral is independent of q so the last two integrals can be performed sequentially. These last two integrals are independent of x and t and so amount to a mere prefactor[2], call it Q. The first integral does depend on the observable coordinate and is but a definition of the Airy function in the reals,

$$\int_{-\infty}^{\infty} \mathrm{d}P\, e^{-\frac{i}{2\mathcal{E}_0}\left(\frac{P^3}{3}+\Pi(x)\,P\right)} = 2\pi(2\,\mathcal{E}_0)^{1/3}\,\mathrm{Ai}\left(\frac{\Pi(x)}{(2\,\mathcal{E}_0)^{2/3}}\right) = 2\pi(2\,\mathcal{E}_0)^{1/3}\,\mathrm{Ai}(\tilde{x}). \qquad (4.28)$$

Recall that the component of the adiabatic wavefunction, Eq. (4.3), corresponding to reflections under the potential barrier was determined to be exactly the function $\mathrm{Ai}(\tilde{x})$. This could be justified by the functional dependence of the Airy functions and proved by the asymptotic expansions of the Airy function for large coordinates x.

---

[2]Note that Q is an incomplete Airy function with its saddle point as a limit. By symmetry arguments, this integral is exactly one half of the full Airy function,

$$Q(\mathcal{E}_0) = \int_{-\infty}^{\infty} \mathrm{d}q\, q\, e^{-\kappa\,|q|} \int_{-\infty}^{t''_0} \mathrm{d}t''\, e^{i\frac{\mathcal{E}_0^2}{2}\left(t''^3/3+\Pi(q)\,t''\right)} = \pi(2\,\mathcal{E}_0)^{1/3} \int_{-\infty}^{\infty} \mathrm{d}q\, q\, e^{-\kappa\,|q|}\,\mathrm{Ai}(\tilde{q}). \qquad (4.27)$$

The remaining integral has analytic solutions but since prefactors are not relevant to this study, this is not explored further.

The exact same conclusion can be drawn here, with the distinction that this identification arises from the definition of a partial contour rather than from a simple superposition of functions. That is, the part of the contour up to the saddle point in P can be directly identified with the part of the wavefunction corresponding under the barrier reflections.

One should take a moment to appreciate how powerful this statement is. It tells us that the physical behaviour of the wavefunction can be understood by analysing the saddle points and corresponding integration contours of the wavefunction integral, *even* when all different contributions are amalgamated in the resultant wavefunction distributions.

4.2.2   Integration from saddle point to observation time

After having observed the connection between the contour to the saddle point and sub-barrier reflections, one can conjecture that the remaining path to the observation time corresponds to transmission. However, since the pathologies introduced by the dependence of the limit on t have been isolated to this contour, one can expect this is somewhat harder to show. Consider the integral

$$\int_{-\infty}^{\infty} \mathrm{d}P \, e^{-\frac{i}{2\mathcal{E}_0}\left(\frac{P^3}{3}+\Pi(x)\,P\right)} \int_{-\infty}^{\infty} \mathrm{d}q \, q \, e^{-\kappa\,|q|} \int_{t_0''}^{P/\mathcal{E}_0} \mathrm{d}t'' \, e^{i\,\frac{\mathcal{E}_0^2}{2}\left(t''^3/3+\Pi(q)\,t''\right)}. \qquad (4.29)$$

One may approximate the integral in t'' by noting that the observation time $t = P/\mathcal{E}_0$ lies on the real line of the complex t'' plane. The saddle point t_0'' has the steepest descent contours running approximately horizontally parallel to the complex plane. Conversely the steepest ascent path lies perpendicular to this and so one may conclude that the point $t = P/\mathcal{E}_0$ always lies above the saddle point t_0'', meaning one may apply the method of Laplace [70] to estimate this integral.

This method relies on the maximum of the integrand lying in between or, as in this case, at one of the end points. This point will be the majour contribution to the integral, thus allowing a simple expansion of the integrand to first order around this maximal point to act as a good approximation. Formally,

$$\int_{t_0''}^{t} \mathrm{d}t'' \, e^{i\,\frac{\mathcal{E}_0^2}{2}\left(t''^3/3+\Pi(q)\,t''\right)} \approx e^{i\,\frac{\mathcal{E}_0^2}{2}\left(t^3/3+\Pi(q)\,t\right)} \int_{t-\varepsilon}^{t} \mathrm{d}t'' \, e^{i\,\frac{\mathcal{E}_0^2}{2}\left(t^2+\Pi(q)\right)(t''-t)}, \qquad (4.30)$$

for some ε. Note the spurious cubic order terms in P, stemming from the coordinate transformation, will be cancelled by those in $t = P/\mathcal{E}_0$, as expected. The last integral in Eq. (4.30) can be handled straightforwardly:

$$\int_{t-\varepsilon}^{t} \mathrm{d}t'' \, e^{i\,\frac{\mathcal{E}_0^2}{2}\left(t^2+\Pi(q)\right)(t''-t)} = \left[\frac{e^{i\,\frac{\mathcal{E}_0^2}{2}\left(t^2+\Pi(q)\right)u}}{i\,\frac{\mathcal{E}_0^2}{2}\left(t^2+\Pi(q)\right)}\right]_{u=\varepsilon}^{u=0} = \frac{2-e^{i\varepsilon\,\frac{\mathcal{E}_0^2}{2}\left(t^2+\Pi(q)\right)}}{i\,\frac{\mathcal{E}_0^2}{2}\left(t^2+\Pi(q)\right)}. \qquad (4.31)$$

It is observed that if the limit $\varepsilon \to i\infty$ is chosen then the error of the estimate is suppressed, as inferred by the Laplace method. With this choice of approximation, and assuming we may interchange the order of integration, the integral wavefunction (4.29) becomes proportional to

$$\int_{-\infty}^{\infty} \mathrm{d}q \, q \, e^{-\kappa |q|} \int_{-\infty}^{\infty} \mathrm{d}P \, \frac{e^{\frac{i}{2\mathcal{E}_0}(\Pi(q)-\Pi(x))P}}{P^2 + \mathcal{E}_0^2 \, \Pi(q)} \tag{4.32}$$

$$= \int_{-\infty}^{\infty} \mathrm{d}q \, q \, e^{-\kappa |q|} \int_{-\infty}^{\infty} \mathrm{d}P \, \frac{e^{i(q-x)P}}{P^2 + \mathcal{E}_0^2 \, \Pi(q)} \tag{4.33}$$

$$= \pi \int_{-\infty}^{\infty} \mathrm{d}q \, q \, e^{-\kappa |q|} \, \frac{e^{-|q-x| \, \sqrt{\Pi(q)}}}{\sqrt{\Pi(q)}}. \tag{4.34}$$

This expression is not further separable and must be calculated numerically. It is however evident, that the x dependence of the wavefunction is of the type $\exp(-k\,x)$ by virtue of the $-|q-x|$ term in the integrand. Thus, one can safely identify this as the transmitted component of the wavefunction.

While the constant field SFA is not a very realistic model, it provides one with a prescription to physically interpret the wavefunction via its defining integral. The main points of this chapter naturally also apply to time dependent fields, although the cost of introducing more complexity translates into a reduced ability to have analytic expressions throughout. In the chapter that follows, the principles derived here are applied to a time dependent electric field to produce a more realistic model. With this model, the causal connection between reflections and the time delay in strong field ionization is then explicitly laid out.

Chapter 5

Ionization in a Time Dependent Laser Field

In the previous chapters, the Wigner time delay was introduced and its appearance was explained as an interference effect between the transmitted and reflected components of the wavefunction under the barrier. This analysis culminated in a method to identify these components by partitioning the wavefunction integral. In this chapter, these principle are applied to the time dependent SFA wavefunction where the same conclusions can be observed for a more realistic ionization scheme.

This chapter is set out as follows: the ionization model within the first order SFA is introduced and the time dependent electron wavefunction calculated. The main features of the wavefunction distribution are explored, in particular those relating to the time delay near the tunnel exit. The emergence of this time delay is again explained by interference effects. To substantiate this, an analytic continuation of the wavefunction integral is performed; the saddle points of this integral allow us to identify transmission and reflection components as paths in the complex plane, as in Chapter 4. When reflection components are extracted from the wavefunction, the wavefunction is shown to have no time delay around the tunnel exit. Lastly, attosecond streaking experiments are discussed, where the distinction between a *measurable* time delay at a detector and time delay around the tunnel exit is emphasised.

The model considered is similar to those of previous chapters: an electron of energy $I_p = \kappa^2/2$, in the bound state

$$\psi_0(x,t) = \sqrt{\kappa} \exp\left(-\kappa|x| + iI_p t\right).$$ (5.1)

of a one dimensional short-range potential,

$$V(x) = -\kappa\,\delta(x).$$ (5.2)

In this case, the electron is ionized by a time-dependent half-cycle laser pulse,

$$\mathcal{E}(t) = -\mathcal{E}_0 \cos^2(\omega t),$$ (5.3)

39

switched on at $\omega t_0 = -\pi/2$.

Since ionization can also happen over-the-barrier (OTBI), a set of parameters is chosen that ensures the physical picture is one of tunnelling. In particular, the Keldysh parameter $\gamma_K = \sqrt{I_p/(2U_p)} \ll 1$ is kept constant. Thus, when varying the field strength $\mathcal{E}_0$, the frequency $\omega = \gamma_K \, \mathcal{E}_0/\kappa$ is varied accordingly. We work in the deep tunnelling regime, where the OTBI threshold[1] is much greater than the electric field strength, $\mathcal{E}_0 \ll \mathcal{E}_{th}$.

This model takes into account all the necessary features of tunnelling ionization. Firstly, ionization occurs mainly in the direction of the electric field so a one dimensional treatment treatment suffices. Likewise, by considering a half-cycle sinusoid laser pulse, electronic recollisions with the atomic core are avoided, simplifying the physical interpretation of the problem. Lastly, the use of a short range potential allows many expressions to be rendered analytically which would otherwise be unfeasible for a pure Coulomb potential.

5.1   Ionization in the Zero Range Potential

As outlined in Chapter 3, the ionization dynamics are described by the Schrödinger equation $i \, \partial_t \Psi(x,t) = (H_0 + H_i)\Psi(x,t)$, with the atomic Hamiltonian $H_0 = -\nabla^2/2 + V(x)$ and the interaction Hamiltonian with the laser field

$$H_i = x \, \mathcal{E}(t). \tag{5.4}$$

The first order SFA wavefunction in 1D is

$$|\psi_i(t)\rangle = -i \int_{-\infty}^{\infty} dp \int_{t_0}^{t} dt' \, |\Psi_p(t)\rangle \, \langle \Psi_p(t')|H_i(t')|\psi_0(t')\rangle. \tag{5.5}$$

The electronic kinetic momentum has been denoted as $\mathcal{P}(t) \equiv p + A(t)$, where $|\Psi_p(t)\rangle = |\mathcal{P}(t)\rangle \, e^{-i \, S(t)}$ are the familiar Gordon-Volkov states in one dimension, with a plane wave component $\langle x \,|\, p \rangle = (2\pi)^{-\frac{1}{2}} \exp(i \, p \, x)$ and Volkov-phase $S(t) = 1/2 \int^t d\tau \, \mathcal{P}(\tau)^2$.

The dipole term takes the form

$$\langle \Psi_p(t')|H_i(t')|\psi_0(t')\rangle = \frac{e^{i(I_p t' - S(t'))}}{\sqrt{2\pi}} \mathcal{E}(t') \int_{-\infty}^{\infty} dx' \, x' \, e^{i \, \mathcal{P}(t')x' - \kappa|x'|} \tag{5.6}$$

which for the moment is kept unevaluated. Instead, consider the representation of the wavefunction in real space

---

[1]This threshold can be estimated as the field strength where the coordinate-saddle point of the SFA-matrix element, i.e. the starting point $x_s \approx \sqrt{\kappa/\mathcal{E}_0}$ of the quantum orbit, becomes comparable to the tunnel exit x_e, which for the short range potential corresponds to the condition $\mathcal{E}_{th} \approx \kappa^3/4$ [72].

$$\psi_i(x,t) = -i\frac{\sqrt{\kappa}}{2\pi} \int_{t_0}^{t} dt' \int_{-\infty}^{\infty} dx' \int_{-\infty}^{\infty} dp \, x' \, \mathcal{E}(t')$$

$$\exp\left[-\kappa|x'| + i\left(\mathcal{P}(t)\,x - \mathcal{P}(t')\,x' + S(t') - S(t) + I_p\,t'\right)\right]. \tag{5.7}$$

Fubini's theorem has been assumed to hold so that the order of integration may be exchanged. The p integration is performed first, yielding

$$\psi_i(x,t) = \int_{t_0}^{t} dt' \int_{-\infty}^{\infty} dx' \frac{x'\sqrt{\kappa}\,\mathcal{E}(t')}{\sqrt{2\pi\,i(t-t')}}\, e^{i\left(I_p t' + i\kappa|x'| + x(A(t)-A(t')) + \frac{i((x-x')-\Delta f_1(t,t'))^2}{2(t-t')} - \frac{\Delta f_2(t,t')}{2}\right)} \tag{5.8}$$

where $\Delta f_n(t,t') = f_n(t) - f_n(t')$ is the difference of integrals of the type

$$f_n(t) = \int^{t} dt' A(t')^n. \tag{5.9}$$

Following x' integration the final analytic expression for the wavefunction is obtained. Defining $z = -i\left(A(t') + (x - \Delta f_1(t,t'))/(t-t')\right)$, $z_\pm \equiv \sqrt{\frac{i}{2}(t-t')}(z\pm\kappa)$ and $\zeta = I_p t' + x\,A(t) + (t-t')((x-\Delta f_1(t,t')^2/(2(t-t')^2) + \kappa^2 + z^2) - \Delta f_2(t,t')/2$ the full time dependent wavefunction takes the form of an integral over t',

$$\psi_i(x,t) = \int_{t_0}^{t} dt' \sqrt{\kappa}\,\mathcal{E}(t')\,e^{i\zeta}\left(\frac{z_-^2(1+\mathrm{Erf}(z_-))e^{-z_+^2}}{z-\kappa} + \frac{z_+^2(1-\mathrm{Erf}(z_+))e^{-z_-^2}}{z+\kappa}\right) \tag{5.10}$$

$$\equiv \int_{t_0}^{t} dt' \exp(i\,\Phi(x,t,t')). \tag{5.11}$$

This is the time integral of the wavefunction which is of interest to this study. It has no analytic solution for finite t and so must be carried out numerically. Traditionally, the saddle point method is employed for large enough observation times t, when the electron is measured at the detector. This method, however, would prevent the study of those times nearest to ionization. The remainder of this chapter will concern the study of this wavefunction integral: firstly, by studying the result of the integration and what it says about ionization time delay and secondly, by analysing the saddle points of the integrand in order to identify, and later extract, the components of this wavefunction corresponding to transmission and reflection.

5.2 Time Delay Near Tunnel Exit

The wavefunction integral (5.10) was integrated numerically using the standard *Mathematica* 12 numerical integration routine (NDSolve) to an accuracy of approximately 30
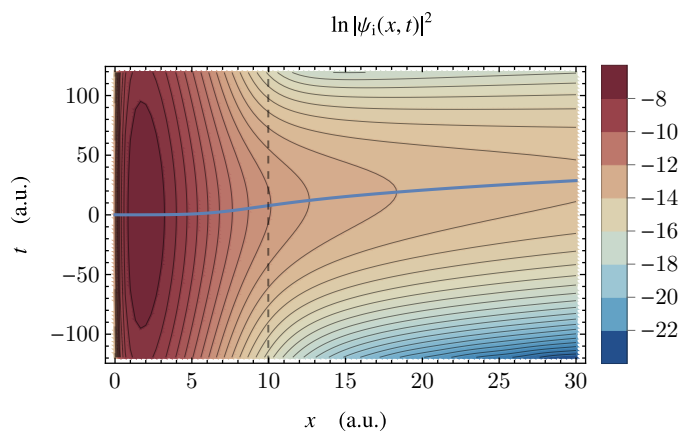
$$\ln |\psi_i(x,t)|^2$$

Figure 5.1:   Ionization amplitude $|\psi_i(x,t)|^2$ as defined in Eq. (5.10). At every cross-section in x, the temporal peak of the wavefunction was determined (plotted in blue) which can be interpreted as the trajectory of the peak.
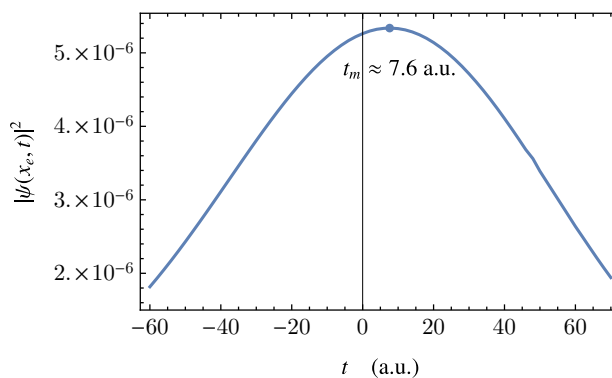

Figure 5.2: Probability distribution $|\psi(x_e,t)|^2$ vs time at the classical tunnel exit $x_e = I_p/\mathcal{E}_0$. This distribution is peaked at a greater time, $t_m \approx 7.6$ a.u. ≈ 183 as, than the peak of the laser pulse.

digits. A field strength $\mathcal{E}_0 = 0.05$ a.u. and Keldysh parameter $\gamma_K = 0.1$ were chosen, to ensure deep tunnelling is considered. Hydrogen, for which $I_p = \kappa^2/2 = 1/2$ a. u., was the chosen atomic species with an OTBI threshold field $\mathcal{E}_{th} \approx 0.25$ a.u.

The resultant space-time probability distribution, $|\psi_i(x,t)|^2$, is plotted in Fig. 5.1. Superimposed is the trajectory of the maximum of the wavefunction, which we term the Wigner trajectory, which is calculated as follows: the temporal probability distribution at each coordinate x is determined (see e.g. Fig. 5.2 for the tunnel exit $x = x_e$) and the peak $t_m(x)$ of this distribution is found. The Wigner trajectory is then the function $t_m(x)$ connecting all the maxima of the space-time probability distribution. This is an analogous concept to the derivative of the phase.

The probability distribution at the classically expected emergence coordinate for the tunnelled electron, $|\psi_i(x_e,t)|^2$, shown in Fig. 5.2, shows that the most likely time of emergence $t_m(x_e) \approx 7.6$ a.u. ≈ 183 as is greater than the peak of laser pulse ($t = 0$). The classical tunnel exit, $x_e = I_p/\mathcal{E}_0$, is is a rough estimate based on a classical picture of tunnelling. In reality, there is not a well defined co-ordinate at which we know the electron would appear, but rather a probability distribution, as shown in Fig. 5.1, dictated by the electron wavefunction. Thus, an appropriate treatment of the tunnelling time should consider a range of co-ordinates and distributions, which is what the Wigner trajectory aims to do.

One advantage of the Wigner trajectory is that it allows a particle interpretation of the electron in the tunnelling region. This allows also for a comparison with the dynamics of a classical electron in the same laser field, as shown in Fig. 5.3.
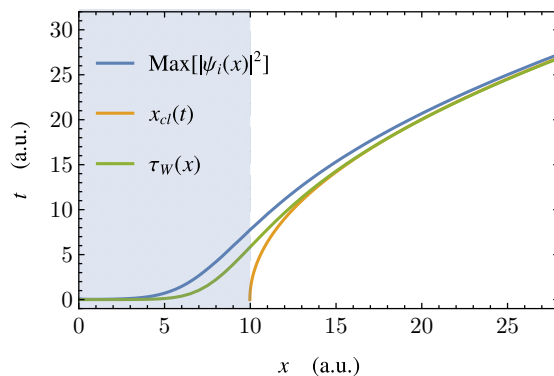

Figure 5.3: Comparison between the peak (blue), classical (orange), and Wigner (green) trajectories in the region near the tunnel exit, x_e. Under the barrier ($x < 10$, shaded blue), there is an increasing delay of the peak w.r.t the laser peak. Over the barrier, the peak trajectory rapidly converges with the classical and Wigner electron trajectory.

Plotted alongside the Wigner and classical trajectories is the Wigner trajectory of the constant field electron as developed in Chapter 4. Under the potential barrier, we see the Wigner that time delay is accrued in the process of tunnelling. Furthermore, all
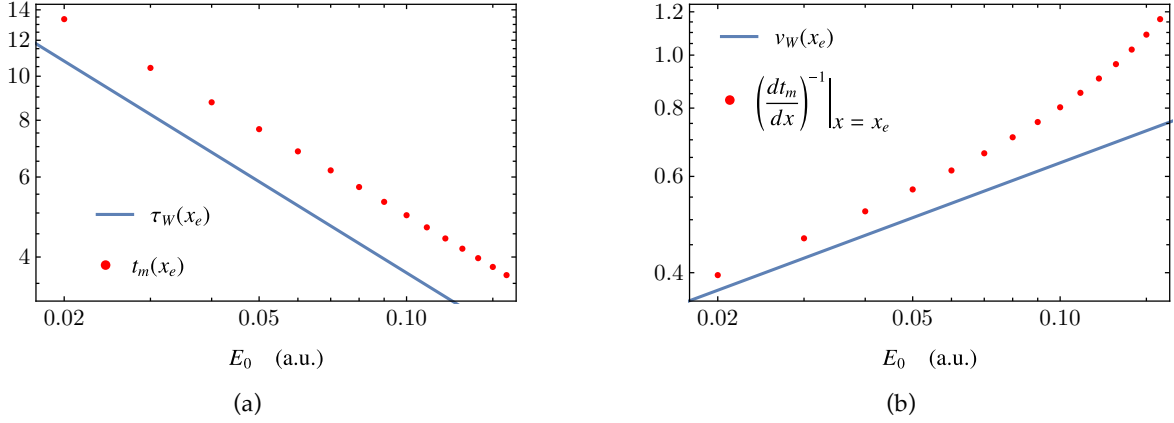
Figure 5.4: Log-log plots of the scaling w.r.t. field strength, $\mathcal{E}_0$, of the (a) Wigner time delay and (b) group velocity at the classical tunnel exit, $x_e = I_p/\mathcal{E}_0$, for the time evolved SFA wavefunction (red dots) and the adiabatic constant field wavefunction (blue lines). For the time evolved wavefunction, the maxima in time, t_m, of the probability distribution $|\psi(x_e, t)|^2$ and its derivative were calculated; for the adiabatic case, results follow from Eqs. (4.5) and (4.6). The agreement in the trends is good, deteriorating as one approaches the OTBI threshold $\mathcal{E}_{th} \approx 0.25$ a.u.

trajectories rapidly become classical in their dynamics; it is expected however, that these trajectories differ somewhat asymptotically since two (Wigner and classical) are time evolved. Moreover, the Wigner trajectory is not calculated via the energy derivative, leading to some difference.

One further application of the SFA wavefunction was in testing the scaling relationships between the tunnelling delay and group velocity derived in Chapter 4. These are compared in Fig. 5.2; the SFA is in good agreement with the adiabatic predictions, up to a proportionality factor. Also evident is the emergence of the OTBI threshold, estimated at $\mathcal{E}_{th} \approx 0.25$ a.u., where the SFA results begin to diverge. This does not negate the validity of the SFA, but rather indicates a change in the physical picture from deep tunnelling to over-the-barrier ionization. At these fields strengths distortions were observed in the probability density rendering obsolete the concept of the peak trajectory.

5.3 The Role of Reflections

The results presented in so far in this chapter assert the existence of a time delay due to the tunnelling process. One main tenet of this thesis is that the interference of transmitted and reflected wavefunction components under a potential barrier generate a time delay, measurable in the peak of the wavefunction. However, in both cases, the separation of reflected and transmitted components was straightforward since the respective wavefunctions were simple superpositions of known functions (namely, exponential
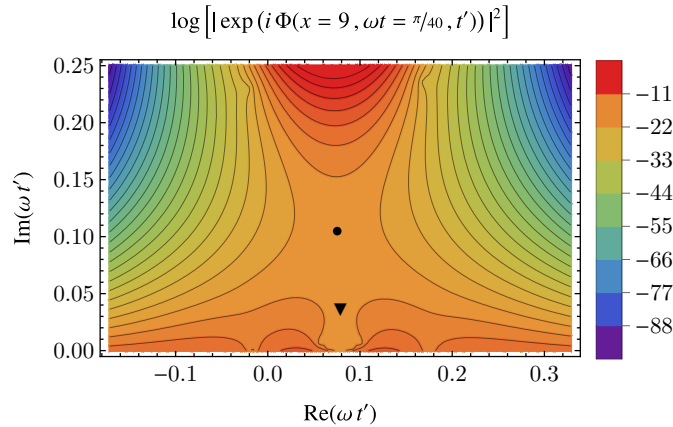
$$\log\left[\left|\exp\left(i\,\Phi(x=9\,,\omega t=\pi/40\,,t')\right)\right|^2\right]$$

Figure 5.5: Complex t' plane of the argument $\Phi(x, t, t')$ of the wavefunction integral $\psi_i = \int_{t_0}^{t} dt' \exp(i\,\Phi)$, for parameters $x = 9$ and $\omega t = \pi/40$. For these configurations there are two saddle-points, denoted by a circle and triangle, the former which, t_+, corresponds to reflections. The saddle-point method can be used to solve the wavefunction integral, when the path is taken over both saddle-points. We use a partial path given by (5.12) to remove the contribution of reflections by integrating over only one of the saddle-points. Other possible configurations of the saddle points are shown in Fig 5.10.

and Airy functions).

On the other hand, the SFA wavefunction presented herein is calculated through an integral where the contributions of transmitted/reflected components are amalgamated and not readily separable. One may very well ask "How can the contributions of reflection/transmission be identified in such a wavefunction?" This question was partially answered already in Chapter 4: there is a significant link between the saddle points of the wavefunction integral and the functional form of the wavefunction i.e. the components of the wavefunction.

Thus, the remainder of this chapter is devoted to the analysis of the saddle points of the wavefunction integral (5.10). It shall be shown that indeed the contributions of reflections can be extracted from the wavefunction and, importantly, when this contribution is neglected the resultant pseudowavefunction displays no time delay.

5.3.1 Analytic Continuation

The integration variable t' is extended into the complex plane and one may then apply principles from complex analysis to integrate the wavefunction integral (5.10). As in Chapter 4, portions of the contour to and from a particular saddle can be assigned physical meaning; partial contour integration going over only the saddle point s_- excludes the the reflections associated with the saddle point s_+.

The same principle is used in the time dependent case; in Fig. 5.5 the complex t' plane for the argument $\Phi(x, t, t')$ is shown for a representative under the barrier con-
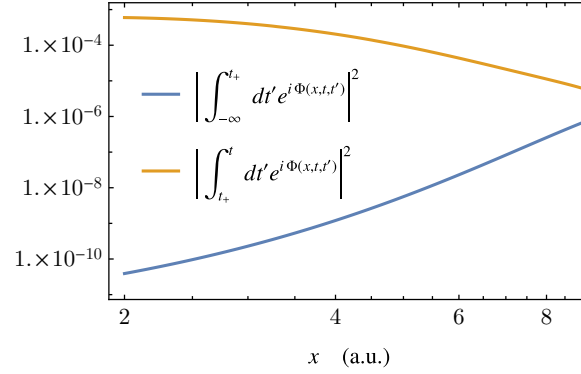
Figure 5.6:   Log-log plot of the relative contributions to the wavefunction amplitude from the portion of the integration path up to the saddle point (blue) and from the saddle point to the given real time $\omega t = 0$ (orange) for various positions x under the classical barrier (i.e. far from the atomic core, but smaller than the tunnel exit). The behaviours are approximately decaying and growing exponentials, respectively, analogous to transmitted and reflected parts of the wavefunction. Similar behaviour is observed at other times, ωt, during the laser pulse.

figuration ($x = 9$, $\omega t = \pi/40$). As in the adiabatic case, two saddle points $t_\pm$, can be identified; ostensibly, these correspond to reflection (t_+) and transmission(t_-) in the time dependent wavefunction.

   To remove the contribution of reflections we seek to avoid the reflection saddle point. This is done by splitting the integration contour is split in two: from negative infinity[2] to the reflection saddle point t_+, and from t_+ (through the saddle point t_-) to the observation time t. The contributions of these two contours to the wavefunction are shown in Fig. 5.6. The first contour contribution grows exponentially under the barrier and can ostensibly be identified as the reflected component; the second decays exponentially, corresponding to the transmitted component of the wavefunction. In this manner, a pseudo-wavefunction can be defined which purposefully neglects contributions from reflections.

   The saddle points are naturally dependent on the two variables of the problem, the position x and observation time t, and the effects of these parameters on the saddles are discussed further on. However, it should be noted that since the orientation of the saddle points in the complex plane changes around the tunnel exit, $x \approx x_e$, the definition of the integration path for the pseudowavefunction necessarily also changes.

   With this in mind, we define the pseudowavefunction neglecting reflections:

---

[2]The lower limit was chosen to be negative infinity rather than the start of the pulse to help numerical convergence. This has no physical effect since the integral is zero for times before the beginning of the pulse.

$$\psi_{nr}(x,t) = \begin{cases} \displaystyle\int_{-\infty}^{t_+} dt' \exp(i\,\Phi(x,t,t')) & x > x_e \\[2em] \displaystyle\int_{t_+}^{t} dt' \exp(i\,\Phi(x,t,t')) & x < x_e. \end{cases} \qquad (5.12)$$

This definition relies on having two saddle points which are distinguishable, at least insofar as their contributions to the integral are separable. The latter no longer holds when cubic terms in an expansion of the argument $\Phi(x,t,t')$ around one saddle point are no longer negligible due to the proximity of the other saddle [73, 74], i.e. if

$$\left| \frac{\frac{\partial^3}{\partial t'^3}\Phi(x,t,t')}{\left(\frac{\partial^2}{\partial t'^2}\Phi(x,t,t')\right)^{\frac{3}{2}}} \right|_{t'=t_\pm} \gtrsim 1. \qquad (5.13)$$

Excluding the above mentioned spacetime coordinates, we may construct a probability distribution from the pseudowavefunction (5.12), as is done in Fig. 5.7. It can be seen that whereas the full SFA wavefunction exhibits a time delay of the order of 5 a.u. with respect to the peak of the pulse at $t = 0$, the same time delay is absent from distribution which neglects reflections.

As before, we may proceed to generate a Wigner trajectory by joining up all such temporal peaks; Figure 5.7 was plotted for $x = 8$ a.u. so as to be as close as possible to the classical tunnel exit, x_e. The restriction given by condition (5.13) implies the existence of an area of the (x,t) plane for which no probability distribution can be meaningfully calculated; this exclusion region is plotted in Fig. 5.9. This region coincides with the classical estimates for the tunnel exit and it is possible in fact to deduce a tunnel exit from the merging of the saddle points, as is done in Sec. 5.4.

The resultant no-reflection Wigner trajectory, with the excluded region left blank, is shown in Fig. 5.8. The extraordinary feature of this figure is that for every distribution inside the tunnelling barrier, shaded in blue, the time delay with respect to the peak of the laser has vanished. This corroborates the hypothesis of this work, that interference of transmitted and reflected components of a wavefunction induce a time delay in the peak (i.e. a Wigner delay). This can be understood as a pure wave phenomenon; if there are no reflected waves then there can be no interference of transmitted and reflected waves and hence the peak of the wavefunction is unaffected by the tunnelling process.

Comparing the no-reflection trajectory with the time evolved SFA and classical trajectories, as in Fig. 5.8, three aspects are worthy of note. Firstly, as already mentioned, the wavefunction without reflections displays no delay under the barrier. Secondly, outside the barrier the trajectory corresponding to this wavefunction quickly becomes classical. This can be understood by the definition Eq. 5.12: as t increases the influence of the second saddle, t_-, diminishes and the wavefunction integral essentially becomes
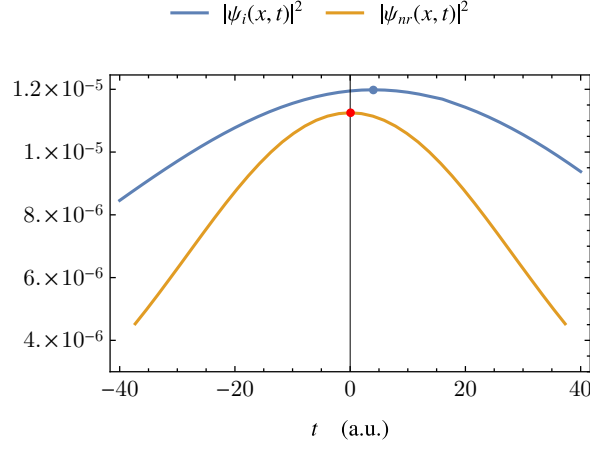
Figure 5.7: Temporal probability distributions at the position $x = 8$ a. u. (under the barrier, near tunnel exit), for the ionized wavefunction, ψ_i, and the pseudo-wavefunction neglecting reflections, ψ_{nr}. The physical wavefunction has accrued a Wigner time delay with respect to the laser field, whereas the maximum of the pseudo-wavefunction is synchronous with the laser field peak.
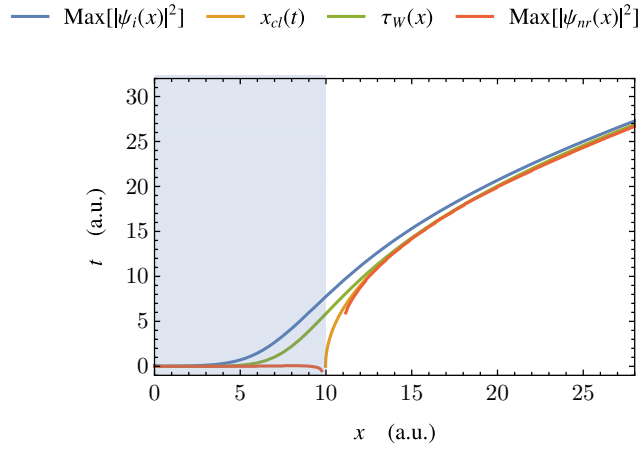
Figure 5.8: Trajectories in the (x, t) plane via: the maximum of the wavefunction ψ_i, the maximum of the wavefunction neglecting reflections ψ_{nr}, and the energy derivative of the constant field wavefunction $\tau_W(x)$. The classical electron trajectory, $x_{cl}(t)$, starting at the tunnel exit at the peak of the laser field is also shown. Under the barrier, the probability distribution neglecting reflections $|\psi_{nr}|^2$ shows zero time delay. In regions where Eq (5.13) does not apply, mostly near the classical tunnel exit, we may not identify reflections nor plot a subsequent trajectory.

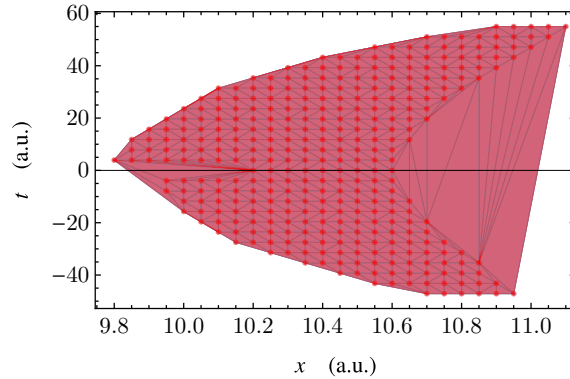Figure 5.9: Region of excluded points in (x, t) parameter space. For points within this region, the pseudowavefunction, ψ_{nr} given by Eq. (5.12), cannot be meaningfully calculated since for these parameter combinations the saddle points of the wavefunction integral, Eq. (5.10), are too close and the contributions of each saddle point (i.e. reflection/transmission) are inseparable.

exactly half of the full time dependent integral Eq. 5.10; this factor of one half only magnitude the magnitude of the integral but not the position of the peak; hence the trajectory becomes classical. Lastly, all trajectories display similar dynamics as the pulse evolves. This suggests that experimentally, for this parameter regime, it is difficult to differentiate between these descriptions at an infinitely distant detector [3]. This difference between interpreted delay at a detector (which depends on the modelling of the electron trajectory) and delay around the tunnel exit is explored further in Section 5.5.

5.4 Tunnel Exit from Saddle Points

The saddle point analysis of Eq. (5.10) may also be used to extract relevant physical information about the electron dynamics. In analogy to the constant field scenario, the topology of complex t' plane reveals the functional behaviour of the electronic wavepacket. The configurations of the saddle points of the argument $\Phi(x, t, t')$ of the wavefunction integral $\psi_i = \int_{t_0}^{t} dt' \exp(i \, \Phi)$ in complex t' plane are presented as a table in Fig. 5.10 . The laser pulse evolves from left to right in this figure and mostly shifts the reference line around which the saddle points are centred, namely $\text{Re}[\omega \, t'] = \omega \, t$. It should be noted, by the definition in Eq. 5.10, a singularity is always to be observed at the point $t' = t$. As one moves down the table of plots, configurations of the complex t' plane are shown for spatial coordinates inside, neighbouring, and outside the tunnelling barrier ($x = 7, 10,$

---

[3]This is not to say that all trajectories in Fig. 5.8 converge at large distances but rather that their dynamics are equivalent and changing parameters such as the classical tunnel exit or the matching point for the adiabatic wavefunction can make these trajectories converge at infinitiy. This sort of backpropagation was explored but is not discussed further in this work.
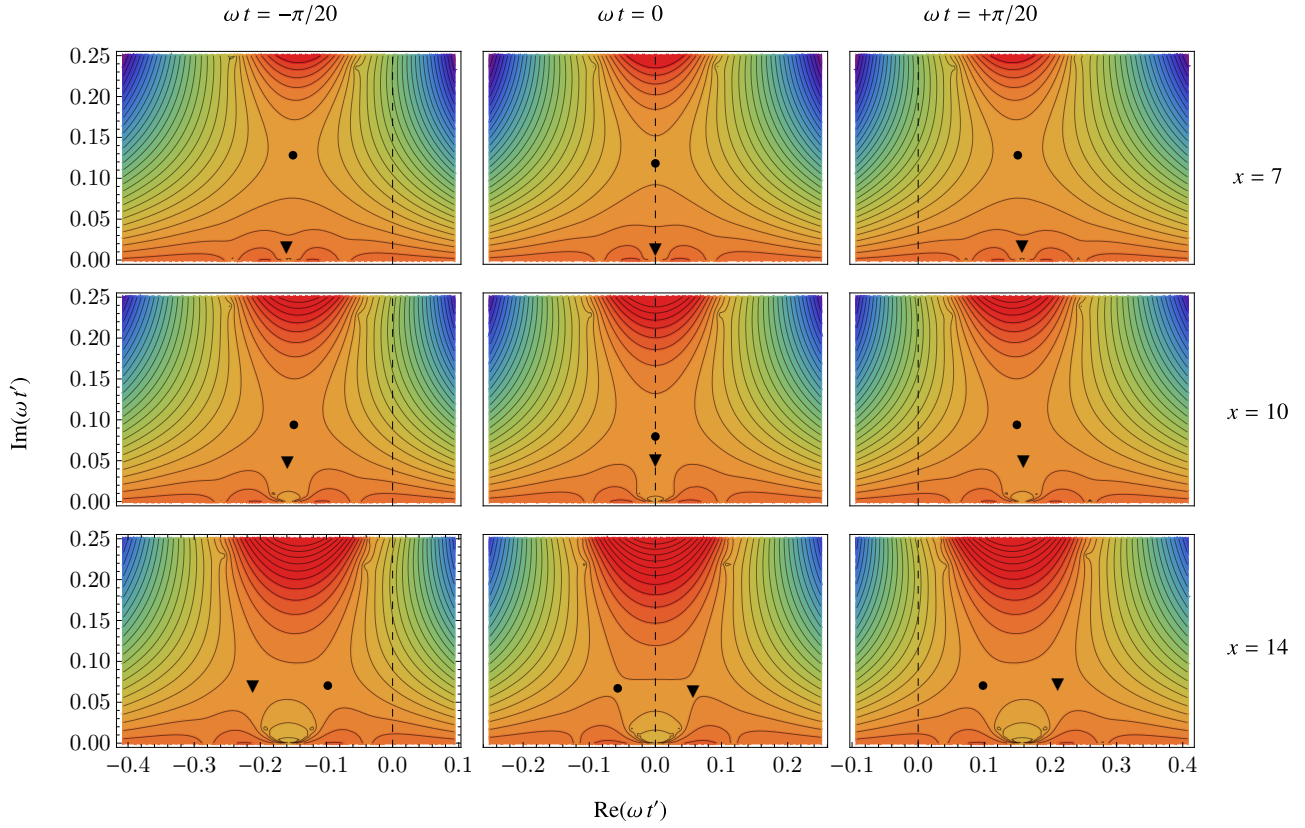
Figure 5.10: Configurations of the saddle points of the argument $\Phi(x, t, t')$ of the wave-function integral $\psi_i = \int_{t_0}^{t} dt' \exp(i\,\Phi)$ in complex t' plane, for parameter ranges $x = 7, 10, 14$ and $\omega t = -\pi/20, 0, +\pi, 20$. The dashed line corresponds to $t' = 0$ and each plot is centred around the (scaled) observation time ωt. The scale and colour coding are identical to those of Fig. 5.5. As x increases the two saddle points approach vertically and, after a closest approach, separate horizontally. For the peak of the pulse, $\omega t = 0$, this closest approach is zero and the two saddle points merge at the point x_t. Otherwise, varying t skews the relative orientation of the saddle points around the line $\mathrm{Re}[t'] = t$.

Figure 5.11: Positions of the upper and lower saddle-points of the integral (5.10) in the complex t' plane with varying x and for fixed $\omega t =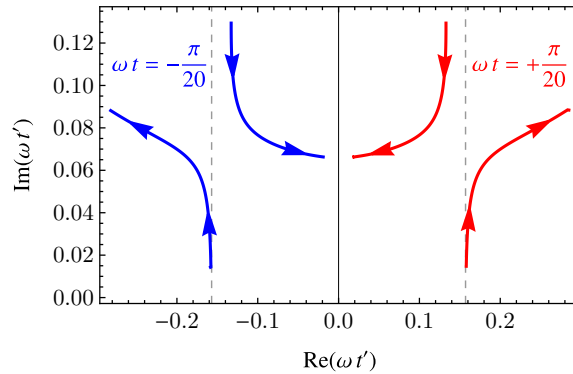 \pm 0.1\pi/2$ (blue and red, respectively). The saddles draw smooth curves with varying x, where the arrows indicate growing values of x. For values of $x \lesssim 7$, the lower saddle-point disappears below the imaginary axis. Each pair of curves is centred around the line $\text{Re}(\omega t') = \omega t$, shown in dashed. For the case $\omega t = 0$, not shown, the two lines meet one point corresponding to $x = x_t$.

and 14 a.u. respectively). There are marked differences between each observation coordinate but the behaviour is reminiscent of the complex plane configuration for the Airy integral, displayed in Fig. 4.2. Indeed, the two pictures can easily be reconciled by a $\pi/2$ rad. clockwise rotation.

Inside the barrier, the saddle points are vertically aligned along the line $\text{Re}[\omega t'] = \omega t$. As one increases the observation coordinate and approaches the tunnel exit, $x \approx 10$, the two saddle points approach each other vertically; as one exits the region neighbouring the tunnel exit, $x \gg 10$, the saddles then separate from each other on the horizontal. This behaviour is shown also in Fig. 5.11. As one approaches the peak of the laser field, $\omega t = 0$, the distance of closest approach around the tunnel exit shrinks. *At the exact peak of the field*, this distance is zero; that is, the saddle points merge. This is directly comparable to the merging of saddle points for the Airy integral at the classical tunnel exit, x_e. In that case, the merging occurs at the classical exit, when $\tilde{x} = 0$, and separates evanescence and oscillatory behaviour in the wave function. In fact, the panels in Fig 5.10 closely resemble those corresponding of Figs. 4.2 (b) and (c), only rotated clockwise.

Thus, there exist two lines, $t = 0$ and $x = x_t$, which define separatrices for the topology of the complex plane and thus the wavefunction. The identification the exact value of x_t is in principle achievable by a binary search or global minimization of the distance function for the saddle points. However, such precision was deemed unnecessary for the purposes of this work. In our study, for a field strength of $\mathcal{E}_0 = 0.05$ and $\gamma_K = 0.1$, we find that this exit takes the value $x_t \approx 10.2$ a.u.; this is in good agreement with the classically expected tunnel exit $x_e = I_p/\mathcal{E}_0 = 10$ a.u. More precise agreement

is achieved with the probability averaged tunnel exit

$$x_K = \frac{\int dt' \frac{I_p}{|\mathcal{E}(t')|} \exp\left(-\frac{2\kappa^3}{3|\mathcal{E}(t')|}\right)}{\int dt' \exp\left(-\frac{2\kappa^3}{3|\mathcal{E}(t')|}\right)} \approx 10.35 \text{ a.u.,} \tag{5.14}$$

where the integration runs over the whole laser pulse, $[t_0, -t_0]$.

5.5 Asymptotic Time Delay

In conclusion, the emergence of a Wigner time delay during tunnelling and a novel definition of the exit coordinate reveal the need to describe the tunnelling process in ionization in quantum mechanical terms. This has implications for the interpretation of attoclock experiments. This work has unambiguously shown that when tunnelling ionization is the dominant mechanism, the peak of the wavefunction accrues a delay (w.r.t. the laser peak) during ionization.

However, a purely classical electron with zero time delay and exit momentum displays equivalent dynamics and hence would yield a similar signal at a detector. Thus, the time delay obtained by measuring the final momentum, what is termed asymptotic time delay, is dependent on how the electron dynamics are chosen to be modelled backwards in time to the moments of ionization.

Since, in general, one does not have direct access to the electron dynamics during ionization, a model dependence is always introduced in this manner. In References [75,76], the authors use classical equations of motion to "backpropagate" the electron towards the tunnel exit. The authors identify a negative time delay with respect to the peak of the laser field and conclude that there can be no time delay. The resolution to this apparent inconsistency is that a non-quantum mechanical treatment of the electron dynamics will yield a model of ionization with negative, not zero, time delay. This is acceptable in as much as it follows from the limitations imposed by a classical description of a quantum process.

In [28], a quantum mechanical description is taken into account using R-matrix methods, however the tunnelling process is described by the a wavefunction calculated using the saddle point approximation (SPA). This is valid for times $\omega t \sim \omega t_f$, where the end points of integration are far away from the relevant saddle points. As described in this work, during the tunnelling process (i.e. near the peak of the laser pulse, $\omega|t| \approx 0$) a saddle point expansion will not approximate the wavefunction integral. Since the end point of integration lies on a path of steepest ascents from the saddle point around which the expansion is performed (see e.g. Fig. 4.3 and visible in Figs. 5.5 and 5.10 where the end point of integration lies always on the real axis), then the expansion does not capture this contribution to the integral. The authors also find negative time delays and again conclude no time delay; the use of the SPA, corresponds well to classical propagation since after ionization ($\omega t \sim \omega t_f$) the electron dynamics are indeed well described classically and so a negative time delay is to be expected.

To obtain reasonable conclusions from the attoclock experimental set up, it is paramount that the tunnelling process be described quantum mechanically. Moreover, a differentiation between time delay near the ionic core and time delay as measured asymptotically is an important conceptual step.

Chapter 6

Ionization with Rescattering Processes

The analysis of ionization so far has been considered only within the scope of direct tunnelling, i.e. only to first order in the SFA. This is justified as the the direct ionization term contributes the most to the integral, and each subsequent term is exponentially suppressed. However, there are also higher orders which may have a small, but visible, effect on the ionization. The purpose of this chapter is to elucidate some of the concepts and difficulties arising from the study of the tunnelling to higher orders, with a view to future work. Second order processes are taken into account and are shown to be subordinate to the first order SFA. Since the magnitude of each term in the SFA series decreases, this effect is limited. The ionization amplitude in the second order SFA can be derived from expression (3.31),

$$\tilde{m}_2(\mathbf{p}) = - \int_{t_i}^{t_f} dt_1 \int_{t_1}^{\infty} dt_2 \int_{-\infty}^{\infty} d\mathbf{p_2} \, \langle \Psi_{\mathbf{p}}(t_1)|V|\Psi_{\mathbf{p_2}}(t_1)\rangle \, \langle \Psi_{\mathbf{p_2}}(t_2)|H_l(t_2)|\psi_a(t_2)\rangle \,, \quad (6.1)$$

after substitution of the field operators, $U_f(t,t') = \int d\boldsymbol{q} \, |\Psi_{\boldsymbol{q}}(t)\rangle \, \langle\Psi_{\boldsymbol{q}}(t')|$ (introduced in Section 3.1). Consider the rescattering term in the one dimensional zero range potential of the previous chapters:

$$\langle \Psi_{\boldsymbol{p}}(t_1)|V|\Psi_{\boldsymbol{p}}(t_1)\rangle = \int_{-\infty}^{\infty} dy \, \langle \Psi_{\boldsymbol{p}}(t_1)|y\rangle \, \kappa \, \delta(y) \, \langle y|\Psi_{\boldsymbol{p}}(t_1)\rangle = \kappa/(2\pi). \quad (6.2)$$

The Born series expansions of scattering waves is valid only for $|V| \ll \hbar^2/(m_e a^2)$ [77], where a is the order of magnitude of the dimensions in which the field differs significantly from zero. The term $\hbar^2/(m_e a^2)$ is of the order of the kinetic energy of the electron in a volume of dimension a. That is, the correction to the incident wave from the effects of the potential must be small [55, 64]. A cursory analysis of Eq. (6.2) reveals that this is not the case. To rectify this issue, a procedure known as the Low Frequency Approximation is performed.

6.1 The Low Frequency Approximation

The Low Frequency Approximation (LFA) [78, 79] essentially removes the effect of the driving laser field on the scattering electron by effecting the substitution,

$$\langle \Psi_{\mathbf{p}}(t_1)| \rightarrow e^{iS(t_1)} \langle \psi_{sc}(\boldsymbol{\mathcal{P}}(t_1))| \tag{6.3}$$

in the second order SFA term, where $|\psi_{sc}(\boldsymbol{\mathcal{P}})\rangle = |\psi_{sc}(\mathbf{p} + \mathbf{A}(t_1))\rangle$ is the scattering state of the electron in the potential V. A derivation of the LFA can be found in [78]; it employs the exact transition matrix, or T matrix, for the field free electron and treats the laser field as the perturbation. In particular, it is valid when the laser period is much larger than the scattering time, whence the name. In the LFA, the amplitude including "recollisions" with the core is then well approximated by the integral:

$$m_2(\mathbf{p}) \approx - \int_{t_i}^{t_f} \mathrm{d}t_1 \int_{-\infty}^{\infty} \mathrm{d}\mathbf{p}_2 \, e^{iS(t_1)} \langle \psi_{sc}(\mathbf{p}) \,|\, V \,|\, \Psi_{\mathbf{p}_2}(t_1) \rangle \int_{t_1}^{t} \mathrm{d}t_2 \, \langle \Psi_{\mathbf{p}_2}(t_2) \,|\, H_{\mathrm{int}}(t_2) \,|\, \psi_a(t_2) \rangle . \tag{6.4}$$

This is a formidable integral to tackle, in particular once the overlaps are taken into account. The same desire to study only the essential picture of ionization leads us to consider a similar one dimensional model of ionization with a short range potential. As before, to avoid multicycle effects (which can generate interference between electron trajectories of the same energy but arising from different cycles), a half-cycle laser pulse will be employed. This means the electron cannot be driven back towards its parent ion after ionization, as the field never changes orientation. In this context, what do recollisions mean?

6.2 Under the barrier recollisions

What is being considered is in fact the effect of a higher order interaction with the core during tunnelling. These effects are known as under-the-barrier recollisons [68]. They account for the reflection of an electron from the surface of the barrier, and the subsequent scattering against ionic the core. This is illustrated in Fig. 6.1.

This can be seen by considering the one dimensional quasi-static limit, c.f. Chapter 4, where $\mathcal{E}(t) \approx -\mathcal{E}_0$ and $V(x) = \kappa\,\delta(x)$ (the reader may refer to Sec. 3.3 for expressions for the bound and scattering states). In this case, the first overlap is

$$\langle \Psi_{p_2}(t_2) \,|\, H_l(t_2) \,|\, \psi_a(t_2) \rangle = \frac{\kappa}{\sqrt{2\pi}} \int_{-\infty}^{\infty} \mathrm{d}y \, e^{i(S(t_2)+\mathcal{P}_2(t_2)y)} \, (-\mathcal{E}_0) \, e^{-\kappa|y|+iI_p t_2} \tag{6.5}$$

$$= \frac{-\mathcal{E}_0\,\kappa}{\sqrt{2\pi}} \left(\frac{2\kappa}{\mathcal{P}_2(t_2)^2 + \kappa^2} \right) e^{i(S(t_2)+iI_p t_2)}, \tag{6.6}$$
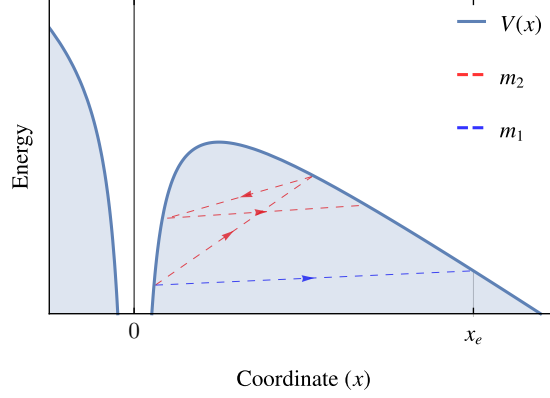
Figure 6.1: Schematic of the under the barrier trajectories for direct (blue) and one-time recollision (red) ionization, given by the amplitudes $m_1(p)$ and $m_2(p)$ respectively. This picture can be understood by studying the saddle points of the integral (6.4). Adapted from [68].

where $\mathcal{P}_2(t) = p_2 + A(t)$, as before. The second overlap is then

$$e^{iS(t_1)} \langle \psi_{sc}(\mathcal{P}(t_1)) \,|\, V \,|\, \Psi_{p_2}(t_1) \rangle = \frac{\kappa}{\sqrt{2\pi}} \int_{-\infty}^{\infty} dy \, \frac{e^{i(S(p,t_1)+\mathcal{P}(t_2)y)}}{1 + i/\mathcal{P}(t_1)} \, \delta(y) \, e^{-i(S(p_2,t_1)+\mathcal{P}_2(t_2)y)} \tag{6.7}$$

$$= \frac{\kappa}{\sqrt{2\pi}} \left(\frac{1}{1 + i/\mathcal{P}(t_1)} \right) e^{i(S(p,t_1)-S(p_2,t_1))}. \tag{6.8}$$

Note, it is now necessary to distinguish between the Volkov phases for asymptotic (p) and rescattering (p_2) momenta. It can be seen that in the full triple integral (6.4) the contribution from the phases of these overlaps will dominate the integrals so saddle point methods approximate the integral well. Denoting the saddle points for the p_2, t_1 and t_2 integrals as p_s, t_i, and t_r, the saddle points of the integral (6.4) are given by the equations

$$p_s = -\frac{\mathcal{E}_0}{2}(t_r + t_i), \tag{6.9}$$

$$I_p = \frac{1}{2}(p_s + \mathcal{E}_0 \, t_i)^2, \tag{6.10}$$

$$\frac{1}{2}(p + \mathcal{E}_0 \, t_r)^2 = \frac{1}{2}(p_s + \mathcal{E}_0 \, t_r)^2. \tag{6.11}$$

This system of equations is solved for the saddle points. There is more than one solution but the only solution leading to physical probabilities is given by

$$p_s = p - 2i\kappa, \qquad \mathcal{E}_0 \, t_i = -p + 3i\kappa, \qquad \text{and} \qquad \mathcal{E}_0 \, t_r = -p + i\kappa. \tag{6.12}$$

By analysis of the integral (6.4), the saddle points t_i and t_r can be interpreted as the initial ionization and recollision times, hence the suggestive labelling. Likewise, p_s can be interpreted as the recollision momentum. For a given momentum, p, these equations define a trajectory in recollision momentum p_s,

$$x(t) = \int_{t_i}^{t} dt' \, \mathcal{P}_s(t') = \int_{t_i}^{t} dt' \, p_s + \mathcal{E}_0 t' = i\kappa(t - t_i) + \frac{\mathcal{E}_0}{2}(t - t_i)^2. \qquad (6.13)$$

For each momentum p, the electron trajectory is interpreted as follows: tunnelling begins at time t_i from the atomic core at $x(t_i) = 0$. The electron tunnels through the potential, arriving at the tunnel exit, $x_e = I_p/\mathcal{E}_0$ at the time $t = 2i\kappa/\mathcal{E}_0$. It is then reflected by the potential barrier, and tunnels again in the opposite direction where it scatters against the core at $x(t_r) = 0$. Here, it reverses its direction yet again and tunnels into the continuum at time $t_e = 0$. This is schematically represented in Fig. 6.1 and forms an intuitive picture of how recollision processes can occur under the potential barrier, in the absence of a multicycle pulse. For each reflection from the barrier, the amplitude m picks up a Keldysh factor of order [68]

$$\exp\left(-\frac{\kappa}{3\mathcal{E}_0}\right). \qquad (6.14)$$

It was shown in Ref. [68] that the interference between direct and recollision terms generated an asymptotic time delay. To understand, however, how under-the-barrier recollisions affect the tunnelling picture around the barrier, it is desirable to calculate the wavefunction $|\psi_r(t)\rangle$ for intermediate times and in a time dependent electric field. This topic is broached in the following section, where the current progress in this direction is discussed.

6.3   The Recollision Amplitude

In this section, we wish to motivate how Eq. (6.4) may be solved. This is done to show how a pathway to the study of under-the-barrier recollisions at the tunnel exit might look like and give a flavour of the difficulties involved. For the 1D short range potential, the recollision amplitude is

$$m_2(p) \approx - \int_{t_i}^{t_f} dt_1 \int_{t_1}^{t_f} dt_2 \int_{-\infty}^{\infty} dp_2 \, e^{iS(t_1)} \langle \psi_{sc}(\mathcal{P}(t_1)) \,|\, V \,|\, \Psi_{p_2}(t_1)\rangle \, \langle \Psi_{p_2}(t_2) \,|\, H_{\text{int}}(t_2) \,|\, \psi_a(t_2)\rangle \,.$$
$$(6.15)$$

The overlaps coincide exactly with expressions (6.5)-(6.8) with the substitution $-\mathcal{E}_0 \to \mathcal{E}(t) = -\mathcal{E}_0 \cos^2(\omega t)$. The integral in p_2 is readily calculable analytically. The double time integral is in principle numerically solvable but, due to the highly oscillatory

nature of the integrand, it remains a computational challenge. Instead, for the time being, we seek to estimate the momentum distribution $|m_2(p)|^2$ by applying the saddle point method to the integral (6.15). The above double integral can be expressed in the form

$$m_2(p) = -\int_{t_i}^{t_f} dt_1\ I(t_1) = \int_{t_i}^{t_f} dt_1\ e^{i\varphi(t_1)} \qquad (6.16)$$

where $I(t_1) = \int_{t_1}^{t_f} dt_2\ f(t_1, t_2)$ is the remaining integral in the recollision time t_2 and $t_f = -t_i = \pi/(2\omega)$ is the end of the laser pulse. To perform the saddle point approximation, the saddle points τ_r of the phase $\varphi(t_1)$ are needed. However, the phase depends on t_1 as a limit of integration so the Leibniz rule applies[1]. Fortunately, the boundary terms in the Leibniz rule vanish for the inner integral so the derivative may be taken directly inside the integral:

$$\frac{\partial \varphi}{\partial t_1} = -i \frac{1}{I(t_1)} \frac{\partial I(t_1)}{\partial t_1}. \qquad (6.17)$$

The saddle points τ_r are the solution to the equation $\varphi'(t_1) = 0$. The saddle point method then provides as an estimate

$$m_2(p) \approx \sqrt{\frac{2\pi}{\varphi''(\tau_r)}}\ e^{i\varphi(\tau_r)} = \sqrt{\frac{2\pi}{\varphi''(\tau_r)}}\ I(\tau_r). \qquad (6.18)$$

The double derivative $\varphi''(t_1)$ may be found by taking the derivative of Eq. (6.17). This saddle point amplitude can easily be calculated in Mathematica. What is numerically harder to find, however, is the relevant saddle point $\tau_r(p)$ around which the approximation is performed. As a first approximation, we may take the saddle point of the constant field, $t_r = 1/\mathcal{E}_0(p - i\kappa)$ given by Eq.(6.12). In this case, we choose to take as the saddle point the solution to the equation

$$p + A(\tau_r) = i\kappa. \qquad (6.19)$$

Even with an approximate saddle point, this method yields faster and more accurate results compared to a problematic brute force calculation of the double integral (6.16). We fix $\omega = \gamma_K/\kappa\mathcal{E}_0$ as before, and take as token parameters $\mathcal{E}_0 = 0.25$ and $\gamma_K = 0.2$. The asymptotic momentum distribution, $|m_2(p)|^2$ is then calculated using the saddle point method given in Eq. (6.18). This is shown in Fig. 6.2, where the exact (i.e. non-saddle-point) first order SFA amplitude, m_1, is introduced for comparison.

---

[1] The Leibniz rule states that

$$\frac{d}{dx}\left(\int_{a(x)}^{b(x)} f(x,t)\,dt\right) = f\big(x, b(x)\big) \cdot \frac{d}{dx} b(x) - f\big(x, a(x)\big) \cdot \frac{d}{dx} a(x) + \int_{a(x)}^{b(x)} \frac{\partial}{\partial x} f(x,t)\,dt.$$
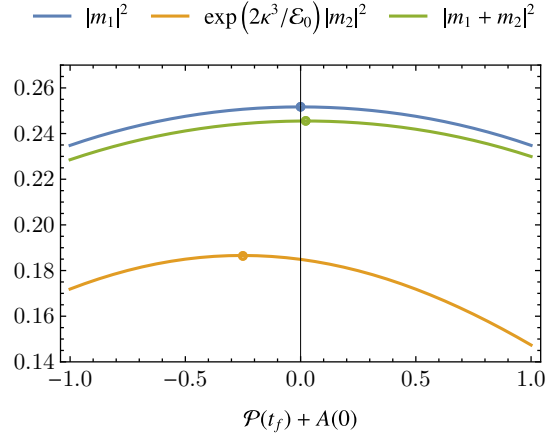
Figure 6.2: The probability amplitudes for direct ionization ($|m_1(p)|^2$, blue), the (scaled) ionization with one recollision ($|m_2(p)|^2$, orange), and their coherent superposition ($|m_1 + m_2|^2$, green) plotted against final momentum $\mathcal{P}(t_f) = p$. The plot is centred around the classically expected value $p = -A(0)$. Dots indicate the maxima.

Two things are noteworthy about this figure. Firstly, it is noted that the recollision distribution $|m_2(p)|^2$ is peaked at negative values of the expected classical momentum $\mathcal{P}(t_f) = p = -A(0)$. This is in contrast to the direction ionization distribution $|m_1(p)|^2$ which is peaked at the classical momentum $-A(0)$. However, their coherent superposition, $|m_1(p) + m_2(p)|^2$ shows a very slight positive peak. This is in agreement with Ref. [68], which first identified that this interference between direct and recolliding amplitudes led to asymptotic time delays and momentums shifts.

Secondly, the tunnelling recollision amplitude, m_2, is suppressed by three barrier interactions (shown in Fig. 6.1) compared to m_1, each time by a factor of $\exp(\kappa^3/3\varepsilon_0)$ as given in Eq. (6.14). The total expected suppression factor is thus $\exp(\kappa^3/\varepsilon_0)$. When $|m_2|^2$ is rescaled by an appropriate factor $\exp(2\kappa^3/\varepsilon_0)$, a good agreement is found with the theory. This corroborates the saddle point method as an appropriate approximation for m_2.

6.4   Outlook

This study motivates further investigation of under the barrier recollisions, and their effects on time delay and momentum shifts around the tunnel exit. It would be desirable to apply the concepts developed elsewhere in this thesis to the second order SFA wavefunction. In particular, an interpretation of the SFA saddle points and contours would be desirable to connect the concept of time delay at the exit (rather than asymptotically, as discussed above and in Ref. [68]).

The above proof of principle outlines the procedure through this may be achieved.

It is doubtful whether the saddle point method remains applicable for intermediate times during the laser pulse, although this is worth investigating. Lastly, any further analysis concerning tunnelling time delay should choose parameters, such as those used in Chapter 5, that ensure tunnelling is the dominant ionization mechanism.

Chapter 7

Conclusions

In conclusion, the time delay phenomenon in ionization was studied in a series of toy models, viz. the square barrier, adiabatic ionization and time independent, as well as time dependent, SFA. In every case, the emergence of a Wigner time delay, i.e. a delay of the peak of the wavepacket due to the barrier, was observed. This time delay was shown to be causally linked to the interference of transmitted and reflected components of the wavefunction.

This was easily demonstrable for the square barrier but more sophisticated methods are required to show the same concept in the SFA. An investigation of the ionization problem in a constant field revealed that the reflected and transmitted components of the wavefunction correspond to parts of the temporal integration contour. In particular, these two contours are divided by a saddle point. By construction of a pseudo-wavefunction neglecting the path corresponding to reflected components, and observing its lack of a Wigner time delay, reflections were shown to be causally linked to the time delay in tunnel ionization. In addition, analysis of the saddle points of the wavefunction integral reveals a new coordinate for the barrier exit grounded not on classical principles but rather on the quantum mechanical SFA wavefunction.

This analysis highlighted the need for such quantum mechanical treatments as the dynamics of the SFA and classical electrons rapidly became indistinguishable as the laser pulse progresses. This brings into focus the distinct concepts of time delay at the barrier exit and asymptotic time delay at a detector. Lastly, the outlook was presented on studying time delay accounting for "under-the-barrier recollisions", a novel concept in studies of strong field ionization.

This work has for the most part implications on how to interpret attoclock data, which is of importance to the calibration of the clock itself. In order to present a clear, unambiguous, picture of tunnelling ionization, approximations and simplifications were made such that only the necessary physics was taken into account. This is, naturally, not the full picture of what happens in attosecond angular streaking experiments. In what follows, these approximations are re-examined and a future outlook is presented on how the conclusions of this work may be applicable in future work.

7.1 Limitations

The assumptions made while composing this work may be broadly divided into physical assumptions and streamlining choices. The former are easily reasoned by considering the typical experimental conditions and making appropriate choices. For example, most attoclock experiments involve ionization where the tunnelled electron is not relativistically accelerated so the dipole approximation (i.e. neglecting magnetic field effects) holds well. The latter were chosen to isolate the problem and distill into it the necessary components: the equations of motion, the choice of potential, and the choice of laser field.

As regards the equations, the SFA is a well established technique that lends itself to simple interpretations. While not explicitly gauge independent, the choice of the length gauge is based on good agreement with numerical TDSE results [65].

Experimentally, there are issues to be taken into account which were not considered. Of these, the laser field is perhaps the most important; laser pulses are multi-cycle, with carrier and envelope waves. One can expect the emergence of carrier-envelope phase effects as well as the interference of ionized electrons with the same momentum but ionized in different parts of the pulse (the so-called long and short trajectories).

Lastly, the choice of potential also plays a role. The zero range potential has been used to describe strong field phenomena such as high harmonic generation [80, 81], above threshold ionization [74, 82], and nonsequential ionization [83] so its use in this work is well justified. The choice of a one dimensional treatment stems from the physical observation that ionization happens principally along the direction of the electric field. Thus, for a theoretical model the 1D zero range potential (ZRP) works well. For comparison with experiment, however, care might have to be taken; the ZRP allows only one bound state so multielectron and depeltion effects are not well modelled by it. In these cases, numerical TDSE methods could again be used as a reasonable comparison.

7.2 Outlook

Due to the limitations of this work, the natural next step would be to apply the concepts developed herein and aim to clarify the calibration of the attoclock. In particular, concepts of time delay, tunnel exit and electron trajectories could in principle be applied to attoclock experimental models. The main underlying difficulty is the numeric nature of very accurate models of ionization, such as the TDSE. This work benefitted greatly from being able to study the saddle points of the wavefunction integral in time. This becomes more challenging when handling models requiring numerical integration, although not impossible. The attoclock method is, in any case, a powerful tool and it promises to open up fruitful avenues of study into atomic and molecular physics.

Appendix A

Atomic Units

Atomic units, first introduced by Hartree [84], are defined by setting three basic units to unity, from which all others are derived. These are typically the reduced Planck constant $\hbar$, the electron mass m_e and the absolute value of the electric charge e. In these units, the speed of light $c \neq 1$ but rather

$$c = \frac{1}{\alpha} = 4\pi\varepsilon_0 \frac{\hbar}{e^2} \approx 137 \text{ a.u.} \tag{A.1}$$

where α is the fine structure constant and $\varepsilon_0 = 1/(4\pi)$ a.u. is the permittivity of free space. The following fundamental quantities, of use when considering atomic systems, are presented in Table A.1 with conversion to SI units with values taken from [60].

Table A.1: Atomic and SI Units Conversion

Quantity	Unit	Significance	Value in SI
Mass	m_e	Electron mass	9.10938×10^{-31} kg
Electric charge	e	Electron charge	1.60218×10^{-19} C
Angular momentum	$\hbar$	Reduced Planck constant	1.05457×10^{-34} J s
Length	$a_0 = \frac{\hbar m_e e}{c\alpha}$	Bohr radius†	5.29177×10^{-11} m
Velocity	$v_0 = \alpha c$	Bohr velocity †	2.18769×10^6 m s^{-1}
Momentum	$m v_0$	Bohr momentum†	1.99285×10^{-24} kg m s^{-1}
Time	a_0/v_0	Bohr period †	2.41888×10^{-17} s
Energy	$\frac{e^2}{4\pi\varepsilon_0 a_0}$	2× Ionization potential H*	4.35974×10^{-18} J
Electric field strength	$\frac{e^2}{4\pi\varepsilon_0 a_0^2}$	Bohr electric field strength†	5.14221×10^{11} Vm^{-1}

† These quantities are understood to pertain to the orbit of an electron in the ground state of the Bohr model of the atom. *Assuming an infinitely massive nucleus.

Appendix B

Time Evolution Operators and the Dyson Equations

In this appendix, the main theory of time evolution operators, and some important identities, are derived, following in the style of the text by Joachain, Klystra and Potvliege [60]. Consider the Schrödinger equation for a state $|\psi\rangle$ in the Schrödinger picture:

$$i\frac{\partial}{\partial t}|\psi(t)\rangle = H(t)|\psi(t)\rangle. \tag{B.1}$$

where the full Hamiltonian may be split into a time independent "free" part and a time dependent interacting part:

$$H(\mathbf{r}, \mathbf{p}, t) = H_0(\mathbf{r}, \mathbf{p}) + H_{\text{int}}(\mathbf{r}, \mathbf{p}, t). \tag{B.2}$$

The evolution operator $U(t, t_i)$ in the Schrödinger picture is defined by

$$|\psi(t)\rangle = U(t, t_i)|\psi(t_i)\rangle \tag{B.3}$$

with the necessary condition $U(t_i, t_i) = \mathbb{1}$. It is a unitary operator with $U(t, t_i) = U^{-1}(t_i, t) = U^{\dagger}(t_i, t)$ which satisfies the Schrödinger-type equation

$$i\frac{\partial}{\partial t}U(t, t_i) = H(t)U(t, t_i). \tag{B.4}$$

This is readily integrable into the equations

$$U(t, t_i) = \mathbb{1} - i\int_{t_i}^{t} H(\tau)U(\tau, t_i)\,\mathrm{d}\tau = \mathbb{1} - i\int_{t_i}^{t} U(t, \tau)H(\tau)\,\mathrm{d}\tau, \tag{B.5}$$

where the second equality stems from the unitarity condition $U(t, t_i) = U(t_i, t)^{\dagger}$.

In the interaction picture one can define the field free evolution operator $U_0(t, t_i)$ corresponding to the free Hamiltonian H_0. It satisfies the same Schrödinger-type equation

$$i\frac{\partial}{\partial t}U_0(t, t_i) = H(t)U_0(t, t_i),\tag{B.6}$$

but as the free field Hamiltonian is time independent this integrates to $U_0(t, t_i) = e^{-i\,H_0(t-t_i)}$, where a similar initial condition $U_0(t_i, t_i) = \mathbb{1}$ applies.

The aim of the interaction picture is to find the evolution operator for the complete Hamiltonian $H(t)$ using the fact that the unperturbed evolution operator $U_0(t, t_i)$ is already known. To this end, define a new state vector in the interaction picture $|\psi_I\rangle$ by the unitary transformation

$$|\psi_I(t)\rangle = U_0^\dagger(t, t_i)\,|\psi(t)\rangle = \exp\left[-\frac{i}{\hbar}H_0(t - t_i)\right]|\psi(t)\rangle\tag{B.7}$$

Since this wavefunction transformation is unitary, all probabilities and observables are unchanged. Note also that at $t = t_i$ the two states, and hence the two representations, coincide, that is $|\psi_I(t_i)\rangle = |\psi(t_i)\rangle$. The Schrödinger equation (B.1) then implies

$$i\hbar\frac{\partial}{\partial t}\,|\psi_I(t)\rangle = U_0^\dagger(t, t_i)\,H_{\text{int}}(t)\,U_0(t, t_i)\,|\psi_I(t)\rangle\tag{B.8}$$

$$\equiv H_{\text{int}}^I(t)\,|\psi_I(t)\rangle\,.\tag{B.9}$$

with the interacting Hamiltonian in the interaction picture

$$H_{\text{int}}^I(t) = U_0^\dagger(t, t_i)H_{\text{int}}(t)U_0(t, t_i).\tag{B.10}$$

Equation (B.8) is known as the Tomonaga-Schwinger equation. It shows that in the interaction picture the time dependence of the state $|\psi_I(t)\rangle$ is caused by the interaction codified in the interaction Hamiltonian $H_{\text{int}}(t)$. Consequently, one can define an evolution operator $U_I(t, t_i)$ in the interaction picture

$$|\psi_I(t)\rangle = U_I(t, t_i)\,|\psi_I(t_i)\rangle\tag{B.11}$$

It can be readily shown that this operator has the properties of a time evolution operator and hence that this definition is not a misnomer. From the Tomonaga-Schwinger equation (B.8) it follows

$$i\hbar\frac{\partial}{\partial t}U_I(t, t_i) = H_{\text{int}}^I(t)\,U_I(t, t_i).\tag{B.12}$$

which can again be integrated to give the integral equations

$$U_I(t, t_i) = \mathbb{1} - i\int_{t_i}^t H_{\text{int}}^I(\tau)\,U_I(\tau, t_i)\,\mathrm{d}\tau = \mathbb{1} - i\int_{t_i}^t U_I(t, \tau)\,H_{\text{int}}^I(\tau)\,\mathrm{d}\tau.\tag{B.13}$$

The link between the Schrödinger and interaction picture evolution operators is deduced from the relations

$$|\psi_I(t)\rangle = U_0^\dagger(t, t_i) \, |\psi(t)\rangle = U_0^\dagger(t, t_i) \, U(t, t_i) \, |\psi(t_i)\rangle \tag{B.14}$$

$$= U_0^\dagger(t, t_i) \, U(t, t_i) \, |\psi_I(t_i)\rangle \tag{B.15}$$

That is,

$$U_I(t, t_i) = U_0^\dagger(t, t_i) \, U(t, t_i), \tag{B.16}$$

and likewise

$$U(t, t_i) = U_0(t, t_i) \, U_I(t, t_i). \tag{B.17}$$

Thus, if one knows the evolution operator $U_0(t, t_i)$ for an unperturbed Hamiltonian H_0 then the problem of finding the full Schrödinger picture evolution operator $U(t, t_i)$ is reduced to merely finding the evolution operator for the interaction picture $U_I(t, t_i)$. Substituting the right–handsides of (B.13) into (B.16) and (B.17) respectively yields the identities

$$U(t, t_i) = U_0(t, t_i) - \frac{i}{\hbar} \int_{t_i}^{t} U_0(t, \tau) \, H_{\text{int}}(\tau) \, U(\tau, t_i) \, \mathrm{d}\tau, \tag{B.18}$$

$$U(t, t_i) = U_0(t, t_i) - \frac{i}{\hbar} \int_{t_i}^{t} U(t, \tau) \, H_{\text{int}}(\tau) \, U_0(\tau, t_i) \, \mathrm{d}\tau, \tag{B.19}$$

where the definition (B.10) is employed. These are the Dyson equations, which allow for perturbative expansions provided judicious choices are made for the separation of free and interaction Hamiltonians.

Note that the placement of the time dependence in the interaction Hamiltonian H_{int} but not in H_0 is not strictly necessary for this derivation. This means only that direct integration of the unperturbed evolution operator no longer holds, $U_0(t, t_i) \neq e^{-i \, H_0 (t - t_i)}$. The only true requirement for this separation to be of any use is that the form of the unperturbed evolution operator $U_0(t, t_i)$ is known beforehand.

Appendix C

The Saddle Point Method

The saddle point method [85] is used to solve integrals of the form

$$I(x) = \int_\gamma \mathrm{d}z \; g(z) \, e^{i\,f(x)\,h(z)} \tag{C.1}$$

where γ is some contour on the complex plane. If one lets

$$h(z) = \phi(u, v) + i\psi(u, v) \qquad\qquad z = u + iv \tag{C.2}$$

then the integral C.6 can be expressed as

$$I(x) = \int_\gamma \mathrm{d}z \; g(z) \, e^{i\,f(x)\,\psi} \, e^{f(x)\phi} \tag{C.3}$$

Note that $e^{i\,f(x)\,\psi}$ is oscillatory and has only unit modulus for all values of $f(x)$, so $\phi(z)$ is the dominant part of the integral (for sufficiently large $f(x)$).

It is known from the theory of complex analysis that the contour γ may be deformed without changing the value of $I(x)$. A specific contour, γ_s, is sought wherein $\phi(z)$ has a global maximum at some point $z_0 = (u_0, v_0)$, and decreases exponentially fast on the contour γ_s the further one is from z_0. This would allow $I(x)$ to be calculated with exponential accuracy.

By the Cauchy-Riemann equations it can be shown that at the stationary points of either $\phi(z)$ and $\psi(z)$ one must have $h'(z) = 0$ and moreover that $\phi(z)$ and $\psi(z)$ are harmonic functions possessing no local extrema: these stationary points are saddle points. The Cauchy-Riemann equations imply these two functions are orthogonal:

$$\nabla\phi \cdot \nabla\psi = 0 \tag{C.4}$$

That is, contours of constant $\phi(z)$ are orthogonal to contours of constant $\psi(z)$ everywhere in the complex plane. Hence, through each saddle point $z_* = (u_*, v_*)$ there are

two contours of $\psi(z)$ with the value $\psi_* = \psi(u_*, v_*)$. By the orthogonality condition, along one of these contours the point $\phi_* = \phi(u_*, v_*)$ is a local (or global) minimum of $\phi(u, v)$ whereas along the other contour ϕ_* is a maximum of $\phi(u, v)$. That is, one contour connects hills with the condition $\phi(u, v) > \phi_*$ (the steepest ascent) whereas the other connects valleys with $\phi(u, v) < \phi_*$ (the steepest descent).

This latter is our choice for the path γ_s and is known, due to condition C.4, as the path of steepest descents. Along this contour

$$h(z) - h(z_0) = \phi(u, v) + i\psi(u, v) - \phi(u_0, v_0) - i\psi(u_0, v_0) = \phi(u, v) - \phi(u_0, v_0) \quad \text{(C.5)}$$

is real and negative. By making a change of variable $-\tau^2 = h(z) - h(z_0)$ the integral $I(x)$ can be calculated using Gaussian integration. Often, it is not possible to calculate $\mathrm{d}z/\mathrm{d}\tau$ and so a series expansion must be employed,

$$I(x) = \int_\gamma \mathrm{d}z \, g(z) \, e^{i \, f(x) \, h(z)} = e^{ih(z_0)} \int_{\gamma_s} \mathrm{d}\tau \frac{\mathrm{d}z}{\mathrm{d}\tau} \, g(z) \, e^{-i \, f(x) \, \tau^2} \quad \text{(C.6)}$$

Often, it is not possible to calculate $\mathrm{d}z/\mathrm{d}\tau$ and so a series expansion must be employed. However, as we move away from the stationary point z_0 on the integration contour γ_s the successive contribution of each term decreases exponentially and so this method approximates excellently the value of $I(x)$.

Bibliography

[1] A. Einstein, "Strahlungs-Emission und Absorption nach der Quantentheorie," *Deutsche Physikalische Gesellschaft* **18** (Jan., 1916) 318–323.
(Cited on page 1.)

[2] A. Einstein, "Zur Quantentheorie der Strahlung," *Physikalische Zeitschrift* **18** (Jan., 1917) 121–128.
(Cited on page 1.)

[3] J. Hecht, "Short history of laser development," *Optical Engineering* **49** no. 9, (2010) 1 – 23. `https://doi.org/10.1117/1.3483597`.
(Cited on page 1.)

[4] T. H. Maiman, "Stimulated Optical Radiation in Ruby," *Nature* **187** no. 4736, (1960) 493–494. `https://doi.org/10.1038/187493a0`.
(Cited on page 1.)

[5] D. Strickland and G. Mourou, "Compression of amplified chirped optical pulses," *Optics Communications* **56** no. 3, (1985) 219–221. `https://www.sciencedirect.com/science/article/pii/0030401885901208`.
(Cited on page 1.)

[6] B. M. Karnakov, V. D. Mur, S. V. Popruzhenko, and V. S. Popov, "Current progress in developing the nonlinear ionization theory of atoms and ions," *Physics-Uspekhi* **58** no. 1, (Jan, 2015) 3–32. `https://doi.org/10.3367/ufne.0185.201501b.0003`.
(Cited on page 2.)

[7] D. Doria, M. Cernaianu, P. Ghenuche, D. Stutman, K. Tanaka, C. Ticos, and C. Ur,
     "Overview of ELI-NP status and laser commissioning experiments with 1 PW
     and 10 PW class-lasers," *Journal of Instrumentation* **15** no. 09, (Sep, 2020)
     C09053–C09053. `https://doi.org/10.1088/1748-0221/15/09/c09053`.
     (Cited on page 2.)

[8] F. J. Merceret, J. G. Ward, D. M. Mach, M. G. Bateman, and J. E. Dye, "On the
     magnitude of the electric field near thunderstorm-associated clouds," *Journal of
     Applied Meteorology and Climatology* **47** no. 1, (Jan., 2008) 240 – 248. `https:`
     `//journals.ametsoc.org/view/journals/apme/47/1/2007jamc1713.1.xml`.
     (Cited on page 2.)

[9] L. V. Keldysh, "Ionization in the field of a strong electromagnetic wave," *Zh. Eksp.
     Teor. Fiz.* **47** (1964) 1945–1957.
     (Cited on pages 2 and 20.)

[10] M. Protopapas, C. H. Keitel, and P. L. Knight, "Atomic physics with super-high
     intensity lasers," *Reports on Progress in Physics* **60** no. 4, (1997) 389.
     (Cited on page 3.)

[11] A. McPherson, G. Gibson, H. Jara, U. Johann, T. S. Luk, I. A. McIntyre, K. Boyer,
     and C. K. Rhodes, "Studies of multiphoton production of vacuum-ultraviolet
     radiation in the rare gases," *J. Opt. Soc. Am. B* **4** no. 4, (Apr, 1987) 595–601.
     `http://josab.osa.org/abstract.cfm?URI=josab-4-4-595`.
     (Cited on page 3.)

[12] M. Ferray, A. L'Huillier, X. F. Li, L. A. Lompre, G. Mainfray, and C. Manus,
     "Multiple-harmonic conversion of 1064 nm radiation in rare gases," *Journal of
     Physics B: Atomic, Molecular and Optical Physics* **21** no. 3, (Feb, 1988) L31–L35.
     `https://doi.org/10.1088/0953-4075/21/3/001`.
     (Cited on page 3.)

[13] D. N. Fittinghoff, P. R. Bolton, B. Chang, and K. C. Kulander, "Observation of
     nonsequential double ionization of helium with optical tunneling," *Phys. Rev.
     Lett.* **69** (Nov, 1992) 2642–2645.
     `https://link.aps.org/doi/10.1103/PhysRevLett.69.2642`.
     (Cited on page 3.)

[14] B. Walker, B. Sheehy, L. F. DiMauro, P. Agostini, K. J. Schafer, and K. C. Kulander,

"Precision measurement of strong field double ionization of helium," *Phys. Rev. Lett.* **73** (Aug, 1994) 1227–1230.
`https://link.aps.org/doi/10.1103/PhysRevLett.73.1227`.
(Cited on page 3.)

[15] L. D. Landau and E. M. Lifshitz, *Mechanics*. Pergamon, Oxford, 1993.
(Cited on page 3.)

[16] P. M. Paul, E. S. Toma, P. Breger, G. Mullot, F. Augé, P. Balcou, H. G. Muller, and P. Agostini, "Observation of a train of attosecond pulses from high harmonic generation," *Science* **292** no. 5522, (2001) 1689–1692,
`https://science.sciencemag.org/content/292/5522/1689.full.pdf`.
`https://science.sciencemag.org/content/292/5522/1689`.
(Cited on page 4.)

[17] M.-C. Chen, C. Mancuso, C. Hernández-García, F. Dollar, B. Galloway, D. Popmintchev, P.-C. Huang, B. Walker, L. Plaja, A. A. Jaroń-Becker, A. Becker, M. M. Murnane, H. C. Kapteyn, and T. Popmintchev, "Generation of bright isolated attosecond soft x-ray pulses driven by multicycle midinfrared lasers," *Proceedings of the National Academy of Sciences* **111** no. 23, (2014) E2361–E2367,
`https://www.pnas.org/content/111/23/E2361.full.pdf`.
`https://www.pnas.org/content/111/23/E2361`.
(Cited on page 4.)

[18] C. M. Maharjan, A. S. Alnaser, X. M. Tong, B. Ulrich, P. Ranitovic, S. Ghimire, Z. Chang, I. V. Litvinyuk, and C. L. Cocke, "Momentum imaging of doubly charged ions of ne and ar in the sequential ionization region," *Phys. Rev. A* **72** (Oct, 2005) 041403. `https://link.aps.org/doi/10.1103/PhysRevA.72.041403`.
(Cited on page 4.)

[19] P. Eckle, M. Smolarski, F. Schlup, J. Biegert, A. Staudte, M. Schöffler, H. G. Muller, R. Dörner, and U. Keller, "Attosecond angular streaking," *Nature Phys.* **4** (2008) 565.
(Cited on pages 4 and 11.)

[20] P. Eckle, A. N. Pfeiffer, C. Cirelli, A. Staudte, R. Dörner, H. G. Muller, M. Büttiker, and U. Keller, "Attosecond Ionization and Tunneling Delay Time Measurements in Helium," *Science* **322** (2008) 1525.
(Cited on pages 4, 5, and 11.)

[21] R. Dörner, V. Mergel, O. Jagutzki, L. Spielberger, J. Ullrich, R. Moshammer, and
     H. Schmidt-Bäcking, "Cold target recoil ion momentum spectroscopy: a
     'momentum microscope' to view atomic collision dynamics," *Physics Reports* **330**
     no. 2, (2000) 95–192.
     `https://www.sciencedirect.com/science/article/pii/S037015739900109X`.
     (Cited on page 4.)

[22] L. Gallmann, C. Cirelli, and U. Keller, "Attosecond science: Recent highlights and
     future trends," *Annual Review of Physical Chemistry* **63** no. 1, (2012) 447–469.
     `https://doi.org/10.1146/annurev-physchem-032511-143702`.
     (Cited on page 5.)

[23] N. Camus, E. Yakaboylu, L. Fechner, M. Klaiber, M. Laux, Y. Mi, K. Z.
     Hatsagortsyan, T. Pfeifer, C. H. Keitel, and R. Moshammer, "Experimental
     evidence for Wigner's tunneling time," *Physical Review Letters* **119** (2017) 23201.
     (Cited on page 5.)

[24] A. N. Pfeiffer, C. Cirelli, M. Smolarski, D. Dimitrovski, M. Abu-samha, L. B.
     Madsen, and U. Keller, "Attoclock reveals natural coordinates of the
     laser-induced tunnelling current flow in atoms," *Nature Phys.* **8** (2012) 76.
     (Cited on pages 5 and 11.)

[25] I. A. Ivanov and A. S. Kheifets, "Strong-field ionization of He by elliptically
     polarized light in attoclock configuration," *Physical Review A* **89** no. 2, (2014)
     21402.
     (Cited on page 5.)

[26] A. S. Landsman and U. Keller, "Tunnelling time in strong field ionisation," *J. Phys.
     B* **47** (2014) 204024.
     (Cited on page 5.)

[27] A. S. Landsman and U. Keller, "Attosecond science and the tunnelling time
     problem," *Phys. Rep.* **547** (2015) 1.
     (Cited on pages 5, 8, and 10.)

[28] L. Torlina, F. Morales, J. Kaushal, I. Ivanov, A. Kheifets, A. Zielinski, A. Scrinzi,
     H. G. Muller, S. Sukiasyan, M. Ivanov, and O. Smirnova, "Interpreting attoclock
     measurements of tunnelling times," *Nat. Phys.* **11** no. 6, (2015) 503–508.
     (Cited on pages 5 and 52.)

[29] A. M. Zheltikov, "Keldysh parameter, photoionization adiabaticity, and the tunneling time," *Phys. Rev. A* **94** (Oct, 2016) 043412.
https://link.aps.org/doi/10.1103/PhysRevA.94.043412.
(Cited on page 5.)

[30] T. Zimmermann, S. Mishra, B. R. Doran, D. F. Gordon, and A. S. Landsman, "Tunneling Time and Weak Measurement in Strong Field Ionization," *Physical Review Letters* **116** no. 23, (Jun, 2016) 233603.
(Cited on page 5.)

[31] M. Yuan, P. Xin, T. Chu, and H. Liu, "Exploring tunneling time by instantaneous ionization rate in strong-field ionization," *Opt. Express* **25** no. 19, (Sep, 2017) 23493–23501.
http://www.opticsexpress.org/abstract.cfm?URI=oe-25-19-23493.
(Cited on page 5.)

[32] D. Sokolovski and E. Akhmatskaya, "No time at the end of the tunnel," *Commun. Phys.* **1** no. 1, (2018) 47.
(Cited on pages 5 and 8.)

[33] U. S. Sainadh, H. Xu, X. Wang, A. Atia-Tul-Noor, W. C. Wallace, N. Douguet, A. Bray, I. Ivanov, K. Bartschat, A. Kheifets, R. T. Sang, and I. V. Litvinyuk, "Attosecond angular streaking and tunnelling time in atomic hydrogen," *Nature* **568** (2019) 75.
(Cited on page 5.)

[34] C. Hofmann, A. S. Landsman, and U. Keller, "Attoclock revisited on electron tunnelling time," *Journal of Modern Optics* **66** no. 10, (2019) 1052–1070.
https://doi.org/10.1080/09500340.2019.1596325.
(Cited on pages 5, 8, and 10.)

[35] M. Han, P. Ge, Y. Fang, X. Yu, Z. Guo, X. Ma, Y. Deng, Q. Gong, and Y. Liu, "Unifying tunneling pictures of strong-field ionization with an improved attoclock," *Phys. Rev. Lett.* **123** (Aug, 2019) 073201.
https://link.aps.org/doi/10.1103/PhysRevLett.123.073201.
(Cited on page 5.)

[36] B. Feuerstein and U. Thumm, "On the computation of momentum distributions within wavepacket propagation calculations," *Journal of Physics B: Atomic,*

Molecular and Optical Physics **36** no. 4, (Feb, 2003) 707–716.
`https://doi.org/10.1088/0953-4075/36/4/305`.
(Cited on page 6.)

[37] X. Wang, J. Tian, and J. H. Eberly, "Extended virtual detector theory for
strong-field atomic ionization," *Phys. Rev. Lett.* **110** (Jun, 2013) 243001.
`https://link.aps.org/doi/10.1103/PhysRevLett.110.243001`.
(Cited on page 6.)

[38] D. B. Canário, M. Klaiber, K. Z. Hatsagortsyan, and C. H. Keitel, "The role of
reflections in the generation of a time delay in strong field ionization,"
`arXiv:2101.08096 [physics.atom-ph]`.
(Cited on page 6.)

[39] A. Peres, *Quantum Theory: Concepts and Methods*. Kluwer Academic Publishers,
Dordrecht, 1995.
(Cited on page 7.)

[40] E. Schrödinger, *Collected Papers on Wave Mechanics*. Chelsea Publishing Company,
New York, 1982.
(Cited on page 7.)

[41] J. S. Briggs and J. M. Rost, "Time dependence in quantum mechanics," *The
European Physical Journal D - Atomic, Molecular, Optical and Plasma Physics* **10** no. 3,
(2000) 311–318. `https://doi.org/10.1007/s100530050554`.
(Cited on page 7.)

[42] J. S. Briggs, "Equivalent emergence of time dependence in classical and quantum
mechanics," *Physical Review A* **91** (May, 2015) 052119.
`https://link.aps.org/doi/10.1103/PhysRevA.91.052119`.
(Cited on page 7.)

[43] A. M. Steiberg, "Experimental issues in quantum-mechanical time measurement,"
in *Time in Quantum Mechanics*, J. G. Muga, R. Mayato, and I. L. Egusquiza, eds.,
vol. 734 of *Lecture Notes in Physics*, p. 333. Springer Berlin / Heidelberg, 2008.
(Cited on page 7.)

[44] A. I. Baz', "Lifetime of intermediate states," *Yad. Fiz.* **4** no. 8, (1966) .

(Cited on page 8.)

[45] V. Rybachenko, "Time of Penetration of a Particle through a Potential Barrier,"
Sov. J. Nucl. Phys. **5** (1967) 635.
(Cited on page 8.)

[46] M. Büttiker, "Larmor precession and the traversal time for tunneling," *Physical Review B* **27** no. 10, (1983) 6178–6188.
(Cited on page 8.)

[47] R. Ramos, D. Spierings, I. Racicot, and A. M. Steinberg, "Measurement of the time spent by a tunnelling atom within the barrier region," *Nature* **583** no. 7817, (2020) 529–532. https://doi.org/10.1038/s41586-020-2490-7.
(Cited on page 9.)

[48] M. Büttiker and R. Landauer, "Traversal time for tunneling," *Phys. Rev. Lett.* **49** (Dec, 1982) 1739–1742.
https://link.aps.org/doi/10.1103/PhysRevLett.49.1739.
(Cited on page 9.)

[49] R. Feynman, A. Hibbs, and D. Styer, *Quantum Mechanics and Path Integrals.* Dover Publications, 2010.
(Cited on page 9.)

[50] N. Yamada, "Speakable and unspeakable in the tunneling time problem," *Physical Review Letters* **83** (Oct, 1999) 3350–3353.
https://link.aps.org/doi/10.1103/PhysRevLett.83.3350.
(Cited on page 10.)

[51] L. Eisenbud, *The Formal Properties of Nuclear Collisions.* PhD thesis, Princeton University, 1948.
(Cited on page 10.)

[52] E. P. Wigner and L. Eisenbud, "Higher Angular Momenta and Long Range Interaction in Resonance Reactions," *Physical Review* **72** no. 1, (1947) 29–41.
(Cited on page 10.)

[53] E. P. Wigner, "Lower limit for the energy derivative of the scattering phase shift,"

Physical Review **98** (Apr, 1955) 145–147.
`https://link.aps.org/doi/10.1103/PhysRev.98.145`.
(Cited on page 10.)

[54] F. T. Smith, "Lifetime matrix in collision theory," *Physical Review* **118** (Apr, 1960)
349–356. `https://link.aps.org/doi/10.1103/PhysRev.118.349`.
(Cited on page 10.)

[55] D. Bohm, *Quantum Theory.* Prentice-Hall, 1951.
(Cited on pages 11, 21, and 55.)

[56] T. E. Hartman, "Tunneling of a wave packet," *Journal of Applied Physics* **33** no. 12,
(1962) 3427–3433, `https://doi.org/10.1063/1.1702424`.
`https://doi.org/10.1063/1.1702424`.
(Cited on page 13.)

[57] E. Pollak, "Quantum Tunneling: The Longer the Path, the Less Time it Takes," *J.
Phys. Chem. Lett.* **8** no. 2, (2017) 352–356.
(Cited on page 13.)

[58] P. C. W. Davies, "Quantum tunneling time," *Am. J. Phys.* **73** (2005) 23.
(Cited on page 13.)

[59] A. D. Bandrauk, F. Fillion-Gourdeau, and E. Lorin, "Atoms and molecules in
intense laser fields: gauge invariance of theory and models," *Journal of Physics B:
Atomic, Molecular and Optical Physics* **46** no. 15, (Jul, 2013) 153001.
`https://doi.org/10.1088/0953-4075/46/15/153001`.
(Cited on page 18.)

[60] C. J. Joachain, N. J. Kylstra, and R. M. Potvliege, *Atoms in Intense Laser Fields*.
Cambridge University Press, 2011.
(Cited on pages 19, 21, 65, and 67.)

[61] W. Gordon, "Der comptoneffekt nach der schrödingerschen theorie," *Zeitschrift
für Physik* **40** no. 1, (Jan, 1926) 117–133. `https://doi.org/10.1007/BF01390840`.
(Cited on page 19.)

[62] D. M. Wolkow, "Über eine Klasse von Lösungen der Diracschen Gleichung," *Z.*

Phys. **94** (1935) 250.
(Cited on page 19.)

[63] H. R. Reiss, *Foundations of the Strong-Field Approximation*, pp. 1–31. Springer Berlin Heidelberg, Berlin, Heidelberg, 2008.
`https://doi.org/10.1007/978-3-540-73794-0_1`.
(Cited on page 20.)

[64] C. J. Joachain, *Quantum Collision Theory*. North-Holland Publishing Company, 1975.
(Cited on pages 21 and 55.)

[65] S. V. Popruzhenko, "Keldysh theory of strong field ionization: history, applications, difficulties and perspectives," *Journal of Physics B: Atomic, Molecular and Optical Physics* **47** no. 20, (Oct, 2014) 204001.
`https://doi.org/10.1088/0953-4075/47/20/204001`.
(Cited on pages 24 and 63.)

[66] F. H. M. Faisal, "Gauge-invariant intense-field approximations to all orders," *Journal of Physics B: Atomic, Molecular and Optical Physics* **40** no. 7, (March, 2007) F145–F155. `https://doi.org/10.1088/0953-4075/40/7/f02`.
(Cited on page 24.)

[67] M. Belloni and R. Robinett, "The infinite well and dirac delta function potentials as pedagogical, mathematical and physical models in quantum mechanics," *Physics Reports* **540** no. 2, (2014) 25–122.
`https://www.sciencedirect.com/science/article/pii/S037015731400043X`.
(Cited on page 25.)

[68] M. Klaiber, K. Z. Hatsagortsyan, and C. H. Keitel, "Under-the-Tunneling-Barrier Recollisions in Strong-Field Ionization," *Physical Review Letters* **120** no. 1, (Jan, 2018) 13201.
(Cited on pages 29, 56, 57, 58, and 60.)

[69] P. M. Morse and H. Feshbach, *Methods of Theoretical Physics*. McGraw-Hill, New York, 1953.
(Cited on pages 29 and 32.)

[70] C. M. Bender and S. A. Orszag, *Advanced mathematical methods for scientists and engineers*. McGraw-Hill Book Company, New York, 1978.
(Cited on pages 32 and 36.)

[71] L. Levey and L. B. Felsen, "On incomplete airy functions and their application to diffraction problems," *Radio Science* **4** no. 10, (1969) 959–969. `https://agupubs.onlinelibrary.wiley.com/doi/abs/10.1029/RS004i010p00959`.
(Cited on page 34.)

[72] M. Klaiber, J. Daněk, E. Yakaboylu, K. Z. Hatsagortsyan, and C. H. Keitel, "Strong-field ionization via a high-order Coulomb-corrected strong-field approximation," *Physical Review A* **95** no. 2, (Feb, 2017) 23403.
(Cited on page 40.)

[73] C. Chester, B. Friedman, and F. Ursell, "An extension of the method of steepest descents," *Mathematical Proceedings of the Cambridge Philosophical Society* **53** no. 3, (1957) 599–611.
(Cited on page 47.)

[74] C. de Morisson Faria, H. Schomerus, and W. Becker, "High-order above-threshold ionization: The uniform approximation and the effect of the binding potential," *Physical Review A* **66** no. 4, (2002) 43413.
(Cited on pages 47 and 63.)

[75] H. Ni, U. Saalmann, and J.-M. Rost, "Tunneling Ionization Time Resolved by Backpropagation," *Physical Review Letters* **117** no. 2, (2016) 23002.
(Cited on page 52.)

[76] H. Ni, U. Saalmann, and J.-M. Rost, "Tunneling exit characteristics from classical backpropagation of an ionized electron wave packet," *Physical Review A* **97** no. 1, (2018) 13426.
(Cited on page 52.)

[77] L. D. Landau and E. M. Lifshitz, *Quantum Mechanics*. Pergamon, Oxford, 1977.
(Cited on page 55.)

[78] A. Čerkić, E. Hasović, D. B. Milošević, and W. Becker, "High-order above-threshold ionization beyond the first-order born approximation," *Phys.*

Rev. A **79** (Mar, 2009) 033413.
https://link.aps.org/doi/10.1103/PhysRevA.79.033413.
(Cited on page 56.)

[79] W. Becker, S. P. Goreslavski, D. B. Milošević, and G. G. Paulus, "Low-energy electron rescattering in laser-induced ionization," *J. Phys. B* **47** no. 20, (2014) 204022.
(Cited on page 56.)

[80] W. Becker, S. Long, and J. K. McIver, "Higher-harmonic production in a model atom with short-range potential," *Physical Review A* **41** no. 7, (1990) 4112–4115.
(Cited on page 63.)

[81] W. Becker, S. Long, and J. K. McIver, "Modeling harmonic generation by a zero-range potential," *Physical Review A* **50** no. 2, (1994) 1540–1560.
(Cited on page 63.)

[82] W. Becker, J. K. McIver, and M. Confer, "Total multiphoton-ionization rates for an extremely short-ranged potential," *Physical Review A* **40** no. 12, (1989) 6904–6912.
(Cited on page 63.)

[83] R. Kopold, W. Becker, H. Rottke, and W. Sandner, "Routes to Nonsequential Double Ionization," *Physical Review Letters* **85** no. 18, (2000) 3781–3784.
(Cited on page 63.)

[84] D. R. Hartree, "The wave mechanics of an atom with a non-coulomb central field. part i. theory and methods," *Mathematical Proceedings of the Cambridge Philosophical Society* **24** no. 1, (1928) 89?110.
(Cited on page 65.)

[85] A. H. Nayfeh, *Introduction to Perturbation Techniques*. John Wiley & Sons, 1993.
(Cited on page 71.)

Acknowledgments

> "And because all things have
> contributed to your advancement,
> you should include all things in your
> gratitude."
>
> ———————————————
>
> Ralph Waldo Emerson

I would first and foremost like to thank my friends and family for their unwavering support.

I would thank also Prof. Christoph Keitel for taking me on as a PhD student in his division. To Karen Hartsagortsyan I offer my gratitude for his supervision, guidance and patience. Similarly, I would also like to thank Michael Klaiber for the many discussions and general support in our research. I thank him also for help with the abstract in German.

I think also my Prof. Björn Malte Schäfer for agreeing to be a referee for this thesis, as well as Prof. Werner Aeschbach and Dr. Robert Moshammer for making my PhD Committee.

Lastly, I thank Michael Quin for his comments and Raad Al-Kohli for his rigorous proof reading and valuable feedback.